https://doi.org/10.1093/plphys/kiad079 PLANT PHYSIOLOGY 2023: 192: 222–239

Plant Physiology®

Research Article

Grain shattering by cell death and fracture in *Eragrostis tef*

Yunqing Yu,[1,*] **Getu Beyene**,[1] **Justin Villmer**,[1] **Keith E. Duncan**,[1] **Hao Hu**,[2] **Toni Johnson**,[1] **Andrew N. Doust**,[2] **Nigel J. Taylor**[1] **and Elizabeth A. Kellogg**[1]

1 Donald Danforth Plant Science Center, 975 North Warson Road, St. Louis, MO 63132, USA
2 Department of Plant Biology, Ecology, and Evolution, Oklahoma State University, Stillwater, OK 74078, USA

*Author for correspondence: yyu@danforthcenter.org
The author responsible for distribution of materials integral to the findings presented in this article in accordance with the policy described in the Instructions for Authors (https://academic.oup.com/plphys/pages/general-instructions) is Yunqing Yu (yyu@danforthcenter.org).

Abstract

Abscission, known as shattering in crop species, is a highly regulated process by which plants shed parts. Although shattering has been studied extensively in cereals and a number of regulatory genes have been identified, much diversity in the process remains to be discovered. Teff (*Eragrostis tef*) is a crop native to Ethiopia that is potentially highly valuable worldwide for its nutritious grain and drought tolerance. Previous work has suggested that grain shattering in *Eragrostis* might have little in common with other cereals. In this study, we characterize the anatomy, cellular structure, and gene regulatory control of the abscission zone (AZ) in *E. tef*. We show that the AZ of *E. tef* is a narrow stalk below the caryopsis, which is common in *Eragrostis* species. X-ray microscopy, scanning electron microscopy, transmission electron microscopy, and immunolocalization of cell wall components showed that the AZ cells are thin walled and break open along with programmed cell death (PCD) at seed maturity, rather than separating between cells as in other studied species. Knockout of *YABBY2/SHATTERING1*, documented to control abscission in several cereals, had no effect on abscission or AZ structure in *E. tef*. RNA sequencing analysis showed that genes related to PCD and cell wall modification are enriched in the AZ at the early seed maturity stage. These data show that *E. tef* drops its seeds using a unique mechanism. Our results provide the groundwork for understanding grain shattering in *Eragrostis* and further improvement of shattering in *E. tef*.

Introduction

Abscission is a common process in which plants detach unwanted organs, such as senescent or damaged leaves, branches, floral parts, and mature fruits and seeds. It is an important response to developmental or environmental cues, allowing relocation of nutrients and energy and avoidance of pathogen infection. Fruit and seed abscission is also essential for propagation and offspring dissemination and establishment (Patterson 2001). In agriculture, fruit/seed abscission, also called shattering, hinders harvest and reduces crop yield, and therefore, reduced or no shattering in fruit/seed crops has been selected by humans through domestication (Dong and Wang 2015; Li and Olsen 2016).

The mechanism of abscission has been studied in diverse plant systems. It generally occurs at the junction of plant organs in pre-programmed cell layers called the abscission zone (AZ). During abscission, cell wall hydrolytic and modifying enzymes are activated, resulting in wall dissolution and cell separation (Roberts et al. 2000; Kim 2014). Elevated gene expression and/or enzymatic activities of endo-1,4-β-glucanases (cellulases), polygalacturonases (PG), xyloglucan endotransglucosylases/hydrolases (XTH), and/or expansins (EXP) are found in leaf, petal, and fruit AZs of a broad set of dicot species (Tucker et al. 1988; Kalaitzis et al. 1995, 1997; del Campillo and Bennett 1996; Gonzalez-Bosch et al. 1997; González-Carranza et al. 2002; Kim et al. 2006;

Received October 18, 2022. Accepted January 11, 2023. Advance access publication February 9, 2023

Open Access

Mishra et al. 2008; Li et al. 2010; Singh et al. 2011; Wu et al. 2012; Merelo et al. 2017; Li et al. 2019), and a few monocots such as oil palm (*Elaeis guineensis*) (Roongsattham et al. 2012). Knockdown or knockout mutants have confirmed the importance of an endo-1,4-β-glucanase in tomato (*Solanum lycopersicum*), and polygalacturonases and EXP10 in Arabidopsis (*Arabidopsis thaliana*) in promoting abscission in leaf, floral organs, and fruit (Brummell et al. 1999; Cho and Cosgrove 2000; González-Carranza et al. 2007; Jiang et al. 2008; Ogawa et al. 2009).

Plant programmed cell death (PCD) may also be involved in abscission. In petal abscission of Yoshino Cherry (*Prunus* × *yedoensis*) and *Delphinium* × *belladonna*, in which petals remain turgid when abscising, PCD indicators including condensed chromatin and DNA degradation were observed in *D. belladonna* but not *P. yedoensis* prior to abscission, suggesting that PCD is involved in the abscission of *D. belladonna* but not *P. yedoensis* (Yamada et al. 2007). PCD also occurs in the AZ of tomato leaf and flower, particularly at the distal side, as shown by irregular nuclear morphology, DNA fragmentation, changes in organelle structure, and increased gene expression and enzymatic activities of nucleases and proteases (Bar-Dror et al. 2011). Increased cysteine protease expression and activity were also detected in the AZ of rose (*Rosa* × *bourboniana*) petals (Tripathi et al. 2009). In addition, silencing S-like RNase *LX* or overexpressing a protein inhibitor of apoptosis both delay petiole abscission induced by deblading and ethylene treatment in tomato (Lers et al. 2006; Bar-Dror et al. 2011), suggesting that PCD contributes to the timing or progression of abscission.

Fruit abscission of the grass family (Poaceae) is of particular interest due to the agronomic value of cereal crops, with AZ development in rice (*Oryza sativa*) being the best characterized. The rice AZ is a thin layer of non-lignified and cytoplasmically dense cells sandwiched between large lignified cells. Most known AZ genes in rice encode transcription factors (TFs) regulating AZ anatomy and lignification during early development, including the MYB TF *SHATTERING4* (*SH4*), BEL1-type homeobox TFs *qSH1* and *SH5*, APETALA2 TF *SHATTERING ABORTION1* (*SHAT1*) and YABBY TF *YAB2/SHATTERING1* (Konishi et al. 2006; Li et al. 2006, 2020; Zhou et al. 2012; Yoon et al. 2014; Lv et al. 2018; Yu and Kellogg 2018). However, AZ anatomy, cell wall lignification, and gene expression patterns of disparate grass species differ from those in rice (Yu et al. 2020b), raising questions of whether abscission occurs through the same regulatory mechanisms. For example, in green millet (*Setaria viridis*), the reduced-shattering mutant *less shattering1* (*les1*) has the same cell anatomy and lignification patterns as the wild type (Mamidi et al. 2020). Similarly, *Non-brittle rachis 1* (*Btr1*) and *Btr2*, the 2 domestication genes responsible for the loss of abscission in cultivated barley (*Hordeum vulgare* L. subsp. *vulgare*), encode proteins with unknown functions, and the AZ of both the shattering wild barley (*H. vulgare* subsp. *spontaneum*) and non-shattering cultivated barley are lignified, although plants with the shattering alleles appear to have thinner walls in the AZ (Pourkheirandish et al. 2015). Consistent with this evidence, the gene regulatory network of the AZ differs among rice, purple false brome (*Brachypodium distachyon*), and *S. viridis*, with little conservation among the genes specifically enriched in the AZ (Yu et al. 2020a). However, 1 gene that may be conserved is *YAB2/SH1*, which regulates AZ development and was selected during domestication in several grass species including sorghum (*Sorghum bicolor*), foxtail millet (*Setaria italica*), and African rice (*Oryza glaberrima* Steud.) (Lin et al. 2012; Doust et al. 2014; Lv et al. 2018; Odonkor et al. 2018).

Teff (*Eragrostis tef*) is an orphan crop in the subfamily Chloridoideae that originated, and is widely cultivated, in Ethiopia. *E. tef* has gained global popularity due to its nutritious and gluten-free grains, and resistance to drought stress. However, its productivity requires improvement (Chanyalew et al. 2019). *E. tef* was documented as non-shattering compared with its wild progenitor *E. pilosa* (Phillips 1995; Ingram and Doyle 2003). However, an AZ does exist in *E. tef* below the caryopsis, a position that appears uniquely derived in *Eragrostis* based on a phylogeny including about 250 grass species (Yu et al. 2020a, 2020b). Here, we show that the AZ below the caryopsis is conserved in the genus *Eragrostis*. We found that the *E. tef* AZ is mechanistically and genetically distinct from that of other studied grasses, with abscission likely involving cell death. Knockout of the conserved shattering gene, *YAB2/SH1*, has no effect on the AZ in *E. tef*, consistent with the unique shattering mechanism in this species.

Results

Abscission below the caryopsis is conserved among *Eragrostis* species

We first addressed whether abscission below the caryopsis in *E. tef* is associated with domestication or if it is characteristic of other related species. We investigated 12 species representing the major clades of *Eragrostis*, a genus of 406 species. We included the distinctive *E. lilliputiana* (formerly *Heterachne gulliveri*) and *E. scabrida* (formerly *Ectrosia scabrida*), as well as the sister species to all others in the genus, *E. cyperoides* (formerly *Cladoraphis cyperoides*) (Barrett et al. 2020). All 12 species have multi-floret spikelets, and except for *E. cyperoides*, the base of their caryopsis is enlarged into unusual thickened chlorophyll-containing tissue. The caryopsis is borne on a triangular stalk that connects it and the base of the filaments with the rachilla (Supplemental Fig. S1). Most species abscise at the same position below the green tissue of the caryopsis (Fig. 1A, Fig. 1, B, E–K, and M). The 2 sister species *E. ciliaris* and *E. tenella* are polymorphic, abscising below the caryopsis and on the rachilla below the floret (Fig. 1, A, B, F, and G). In addition, in many cases, the lemma and palea have their own Azs that break simultaneously with the AZ below the caryopsis, probably facilitating seed dispersal (Fig. 1, E–H, J, K, and M). In our samples, only 2 species, *E. papposa* and *E. tef*, have persistent

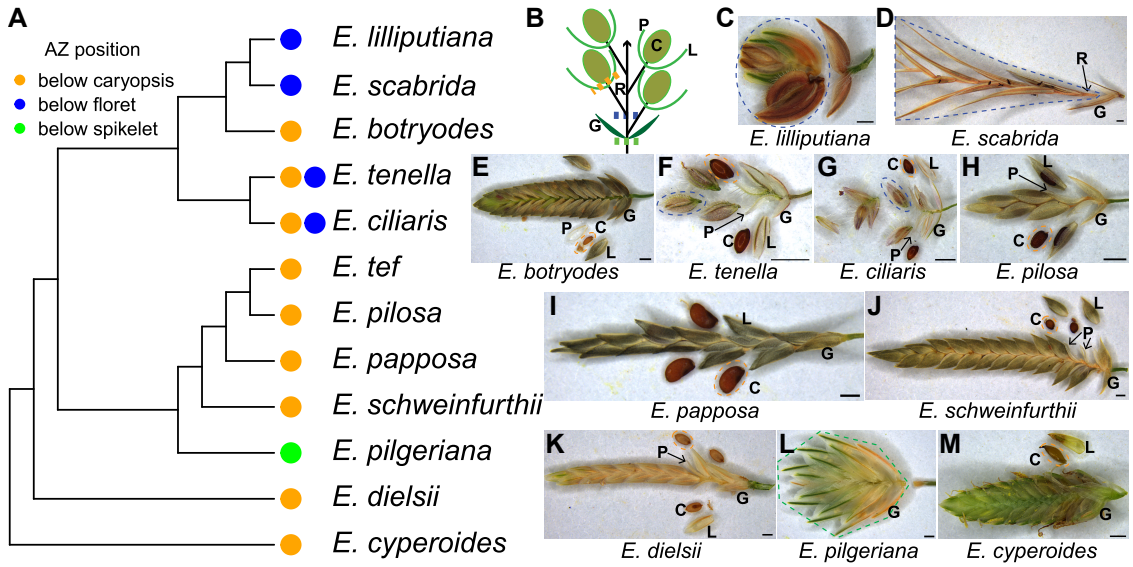

Figure 1 The AZ underneath the caryopsis is common in *Eragrostis*. (A) Dendrogram showing the phylogenetic relationship of the studied species and the AZ position of each. (B) A diagram illustrating the *Eragrostis* spikelet and the possible AZ positions. (C–M) Spikelets of (C) *E. lilliputiana*, (D) *E. scabrida*, (E) *E. botryodes*, (F) *E. tenella*, (G) *E. ciliaris*, (H) *E. pilosa*, (I) *E. papposa*, (J) *E. schweinfurthii*, (K) *E. dielsii*, (L) *E. pilgeriana*, and (M) *E. cyperoides*. The abscised units are circled with dotted lines with the corresponding color shown in (A, B). Scale bars = 0.5 mm. C, caryopsis; G, glumes; L, lemma; P, palea; R, rachilla.

lemmas and paleas at maturity (Fig. 1I, Fig. 2A). Both *E. lilliputiana* and *E. scabrida* abscise below the bottom floret and above the glumes (Fig. 1, A and B–D). An exception among the species is *E. pilgeriana*, which has tough lemmas and paleas and the whole spikelet abscises as a unit (Fig. 1, A, B, and L). Together, these results suggest that the caryopsis as the dispersal unit is largely conserved among *Eragrostis* species and likely originated in the common ancestor of the genus.

A previous phylogenetic study suggests that the ancestral AZ of the grass family and subfamily Chloridoideae is located in the rachilla below the florets (Yu et al. 2020b), and we found 4 species, *E. ciliaris*, *E. tenella*, *E. lilliputiana*, and *E. scabrida* abscise at this ancestral position (Fig. 1, A, C, D, F, and G). Safranin O and fast green staining on these 4 species found that the rachilla AZ resembles a "typical," *Oryza*-like AZ anatomy with non-lignified, small, and flattened cells surrounded by larger cells with or without lignification (Supplemental Fig. S2), suggesting that a typical AZ is retained in some *Eragrostis* species, while it is lost in many others.

Persistent lemmas reduce grain release in *E. tef*

As domesticated *E. tef* shares the same AZ position as its wild progenitor *E. pilosa* and other *Eragrostis* species, and *E. tef* tends to retain its lemma at maturity, we investigated the loss of the lemma AZ as a possible domestication trait (Fig. 2A). We quantified the tensile strength of the lemma in *E. tef* and *E. pilosa* at the seed filling stage when the caryopsis is still attached to the stalk and at maturity when the caryopsis is detached but held in place between the lemma and palea. In both species, lemma tensile strength is lower when the caryopsis is mature, but is consistently and significantly higher in *E. tef* compared with *E. pilosa* at both stages (Student's *t*-test, $P < 0.001$), with 28.6 ± 0.5 gF vs. 20.4 ± 0.3 gF for *E. tef* and *E. pilosa* at seed filling, and 15.9 ± 0.5 gF vs. 1.2 ± 0.1 gF at maturity (Fig. 2B).

Cell structure at the base of the lemma where it detaches at maturity was compared with X-ray microscopy (XRM). Neither species had distinct abscission layers (Fig. 2, C and D), but the base of the lemma was consistently thicker in *E. tef* than in *E. pilosa* (multiple *t*-tests, adjusted $P < 0.05$, Supplemental Table S1A), with larger differences towards the base of the lemma (Slices 1 to 10 vs. 51 to 60, 2-way ANOVA, $P < 0.01$, Supplemental Table S1B; Fig. 2, C–G). In both *E. tef* and *E. pilosa*, safranin O stained epidermal cells and vascular tissues with magenta color, and fast green stained cytoplasm and cellulose, suggesting that the primary and secondary wall proportions at the base of lemma are comparable between the 2 species (Supplemental Fig. S3). These results suggest that the ease of lemma shattering of *E. pilosa* may be attributable to thinner and more fragile lemma tissues rather than a specific AZ, a shattering mechanism not described in other grasses, to our knowledge.

Abscission in *E. tef* is through cell death and physical rupture

We next investigated the caryopsis AZ of *E. tef* as representative of the whole genus. Before abscission, scanning electron microscopy (SEM) showed that the caryopsis is connected to the triangular stalk tissue (Fig. 3, A and D). Manual removal of the stalk left a scar with open cells and a rough surface, as expected (Fig. 3, B and E). The abscission scar of a mature

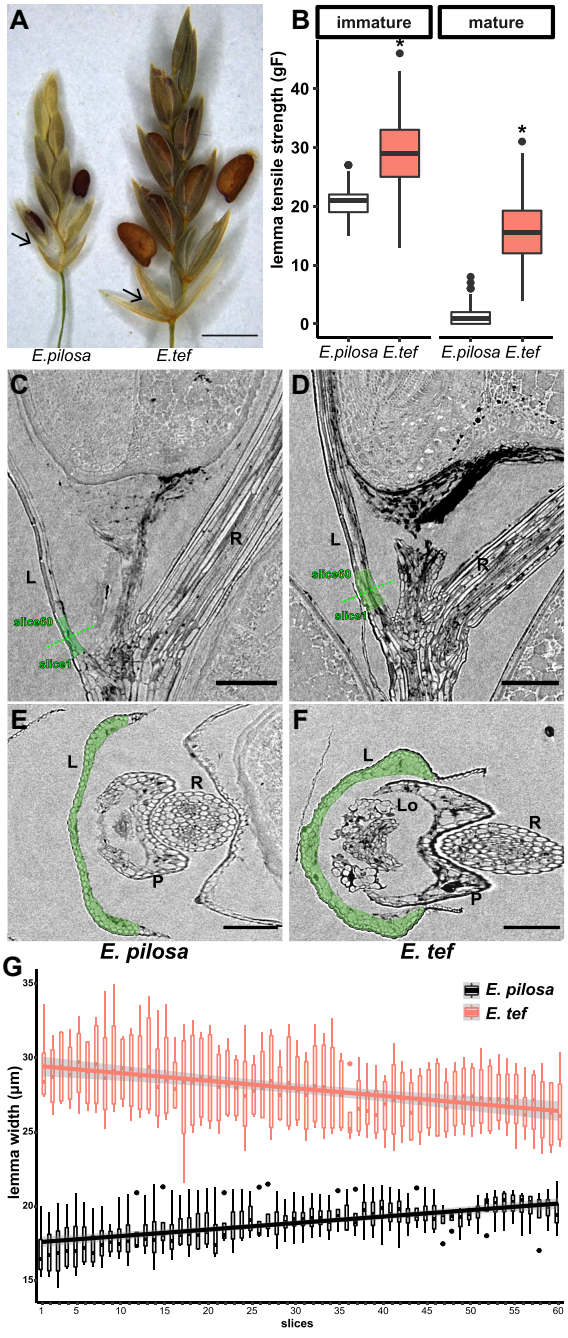

Figure 2 Tough lemma contributes to less shattering of *E. tef* compared with its wild progenitor *E. pilosa*. (A) Lemma of *E. pilosa* shedding with the caryopsis, while the lemma of *E. tef* is retained. Arrows point to the lemma. Scale bar = 1 mm. (B) Tensile strength of lemma at the immature (seed filling) stage and mature stage when the caryopsis has abscised in *E. pilosa* and *E. tef*. Stars denote significant differences (Student's *t*-test, $P < 0.01$) between developmental stages. Values are 120 measurements per genotype per stage from 6 biological replicates. (C–F) X-ray microscope images of (C, E) *E. pilosa* and (D, F) *E. tef*; (C, D) longitudinal and (E, F) cross sections. The green dotted line indicates the position of the cross sections. Scale bars = 100 μm. L, lemma; Lo, lodicule; P, palea; R, rachilla. (G) Lemma width of 60 successive slices in the highlighted green region in (C–F). Width is estimated using area/perimeter*2. Slices 1–60 are from the base to the tip of the lemma. Values are 4 measurements per slice per genotype.

caryopsis that has detached naturally resembles the scar caused by manual rupture, with cells open in the middle (Fig. 3, C and F). Similar patterns were observed in longitudinal slices of XRM images (Fig. 3, G and H). These results suggest that abscission of the *E. tef* caryopsis occurs through physical rupture at the weakest cells rather than by cell separation at the middle lamella.

Transmission electron microscopy (TEM) supports this hypothesis (Fig. 4). At pre-anthesis (s1) and seed filling (s2), the cells are thin walled with dense cytoplasm (Fig. 4, A and B, Supplemental Fig. S4, A and B). However, close to the time of abscission, we observed cells with broken walls that appeared fractured in 3 out of 4 TEM samples (Fig. 4C, Supplemental Fig. S4, C–H). In addition, some cells develop large vacuoles, pushing the organelles to the edge of the cells, and many small vesicles of different sizes were observed, resembling cellular degeneration and cell death (Fig. 4, C and D).

We tested for cell death with trypan blue, which stains dead cells. Post-anthesis anthers and stigmas were stained in all florets, as expected (Fig. 5A), as were the tissues around the AZ at the base of mature caryopses (Fig. 5, C and E). No staining was observed in immature caryopses (Fig. 5, B and D).

The shattering role of *YAB2/SH1* is not conserved in *E. tef*

As *YAB2/SH1* is necessary for AZ development in multiple grass species (Lin et al. 2012; Lv et al. 2018; Li et al. 2020), we tested whether its function is conserved in *E. tef* using *yab2/sh1* knockout mutants generated by CRISPR-Cas9. *E. tef* is tetraploid, and thus most genes exist as 2 homoeologous copies (homoeologs). Using 2 guide RNAs (gRNAs) targeting both homoeologous *YAB2/SH1*, we obtained 3 independent lines, with tetra-allelic mutations, suggesting high editing efficiency at both target sites. In all cases, these mutations generate insertions or deletions leading to frameshift and early stop codons (Supplemental Fig. S5). Caryopsis abscission in the mutants is similar to that in the wild type and empty vector control, suggesting that disrupting *YAB2/SH1* is not sufficient to alter shattering in *E. tef* (Supplemental Fig. S6, A–H). In addition, we found no other obvious phenotypic differences among the genotypes, including lemma tensile strength, inflorescence architecture, or overall morphology (Supplemental Fig. S6, I–K).

To test the hypothesis that there may be natural mutations that lead to malfunction in EtYAB2/SH1, we compared their amino acid sequences with other YAB2 proteins in 6 dicot and 15 monocot species. We focused on the conserved Zinc Finger domain and YABBY domain (Bowman 2000). In the Zinc Finger domain, we found 1 amino acid Alanine at position 45 (alignment position 118, Supplemental Fig. S7) in both homoeologs of EtYAB2/SH1, while all other grass putative SH1 orthologs have a Threonine at this position. However, we found that Alanine is predominant in dicot

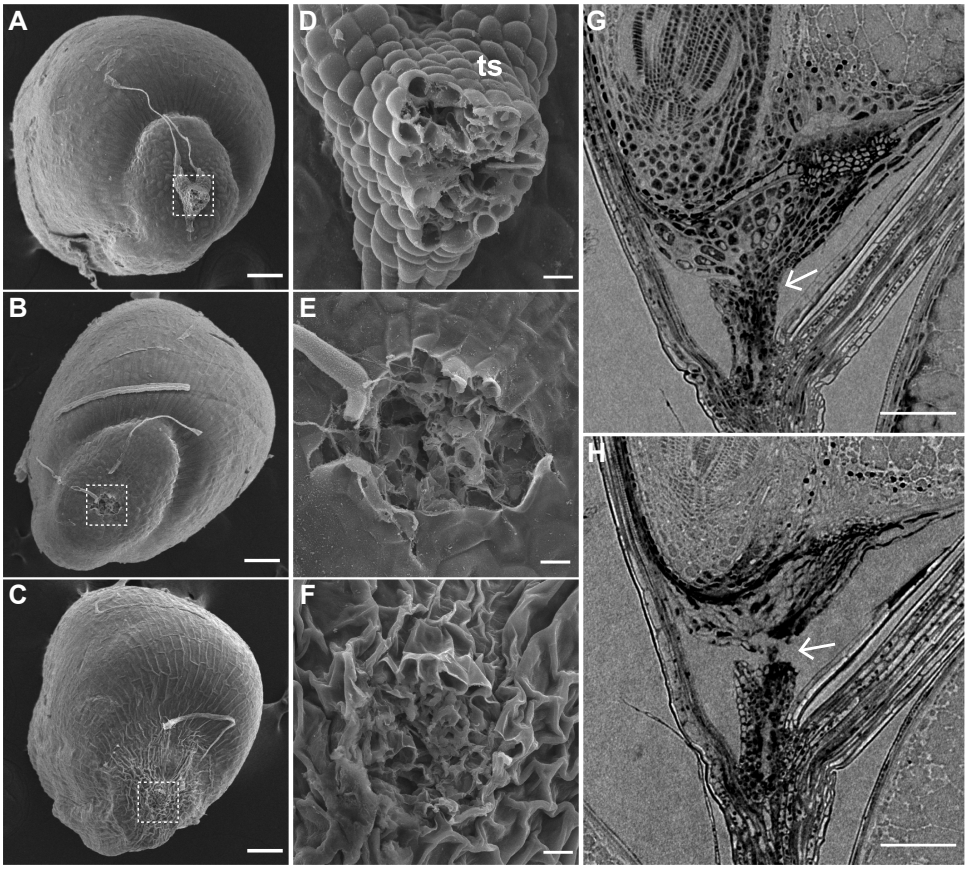

Figure 3 Abscission scar of the caryopsis in *E. tef* has a rough surface. (A–F) SEM images of *E. tef* caryopsis when (A, D) the stalk is attached, (B, E) the stalk is manually removed, and (C, F) the stalk has separated naturally. (A–C) Scale bars = 100 μm. (D–F) Scale bars = 10 μm. (G, H) Longitudinal X-ray microscope images (G) before and (H) after abscission. Arrows point to the AZ. Scale bars = 100 μm. ts, triangular stalk.

YAB2 and also occurs occasionally in other monocot species, suggesting that Alanine 45 is not likely to disrupt the function of EtYAB2/SH1 (Supplemental Fig. S7). In the YABBY domain, we found that Isoleucine at position 117 (alignment position 263) is unique in *E. tef*, as almost all other tested species have a Valine at this position (Supplemental Fig. S7), although these 2 amino acids have similar properties. Together, no obvious deleterious mutations were observed in EtYAB2/SH1.

Genes related to cell death are enriched in the AZ module at the late stage in *E. tef*

To identify genes that are important for AZ development of *E. tef*, we used RNA-Seq to compare the AZ with tissues immediately above (caryopsis) and below (rachilla) it at pre-anthesis (s1), seed filling (s2), and early seed maturity (s3) stages (Supplemental Fig. S8). Weighted Gene Co-expression Network Analysis (WGCNA) was used for identifying genes enriched in the AZ (Langfelder and Horvath 2008). Among the 32 modules identified, 7 are AZ specific, including a single AZ module of 537 genes at s1, 4 AZ modules at s2 with 94, 468, 147, and 406 genes, and 2 AZ modules exclusively at s3 with 2720 and 1715 genes (Fig. 6A, Supplemental Table S2). The gene ontology (GO) categories among different AZ modules were nonoverlapping, except for the 2 modules at s3, suggesting these AZ-enriched genes are stage specific (Fig. 6B, Supplemental Table S3). At s1, the GO term floral organ abscission (GO:0010227) is among the top 10 most significant enriched GO categories (Fig. 6B). Five out of 7 genes in this GO term, including Et_3A_027120, Et_3B_030237, Et_6A_047003, Et_6B_049757, and Et_10A_001133, encode proteins with BTB/POZ domain and ankyrin repeats (Supplemental Fig. S9A). All these BTB proteins share the same Arabidopsis homolog, BLADE ON PETIOLE2, which is involved in petal abscission (McKim et al. 2008).

At s3, GO terms related to organelle organization and senescence are over-represented in the most significant GO of the AZ modules blue and violet (Fig. 6B, Supplemental Table S2), consistent with the TEM observations (Fig. 4, C and D). Both modules share the terms peroxisome organization (GO:0007031), vacuole organization (GO:0007033), membrane fusion (GO:0061025), aging (GO:0007568), and negative regulation of cell death (GO:0060548); 74 and 49 genes are annotated with the latter term in modules blue and violet, respectively. Among these, 10 and 5 genes are also hub genes with the highest 10% connectivity with other

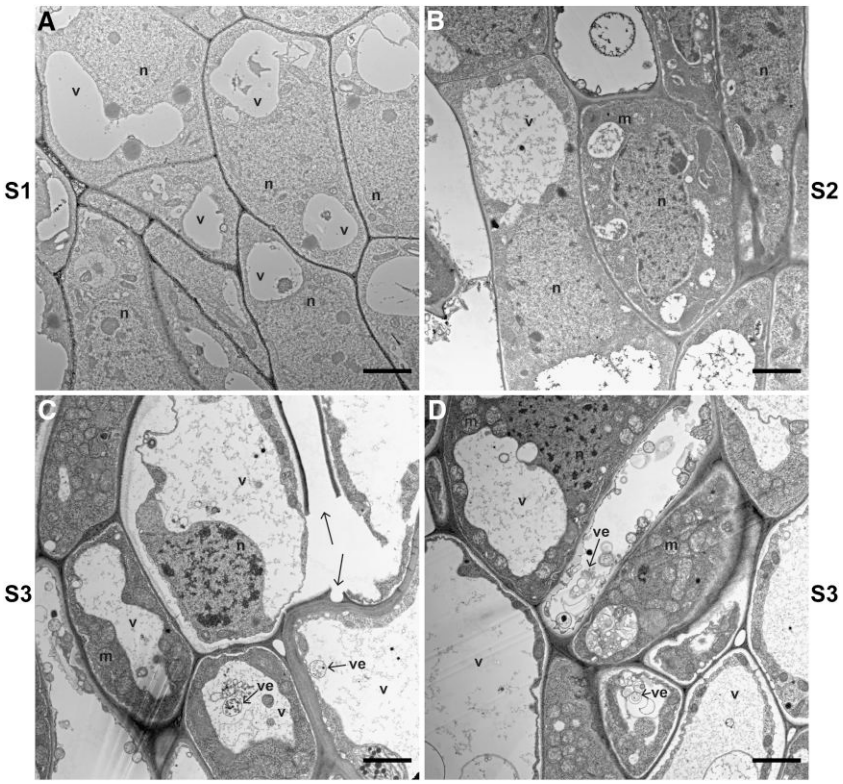

Figure 4 TEM reveals PCD and cell wall breakage in the AZ of *E. tef* at the early seed maturity stage. Images were taken in the AZ (A) before anthesis (s1), (B) at seed filling (s2), and (C, D) at early seed maturity (s3). Arrows point to cell wall breakage and vesicles (ve). Scale bars = 2 μm. m, mitochondrion; n, nucleus; v, vacuole.

genes of the 2 modules (Fig. 6B, Supplemental Fig. S9, B and C, Supplemental Table S4). In addition, module blue is also enriched in the abscisic acid-activated signaling pathway (GO:0009738) and proteasome assembly (GO:0043248), which are known to be involved in PCD (Domínguez and Cejudo 2014).

Genes encoding cell wall hydrolytic and modifying enzymes are enriched in the late developmental AZ

We explored whether cell wall degradation could contribute to abscission through physical rupture. We identified putative cell wall hydrolytic and modifying enzymes based on the Pfam database, including the glycosyl hydrolase family 5 (GH5, cellulase), GH9 (endoglucanase), GH10 (xylanase), XTH, expansin, GH28 (polygalacturonase and rhamnogalacturonase A), pectate lyase, pectin methylesterase (PME), pectin methylesterase inhibitor (PMEI) and pectinacetylesterase (PAE). For each enzyme family, we identified a few genes significantly enriched 2-fold or more in the AZ at s3 and/or in the WGCNA AZ modules at s3 (Fig. 7, Supplemental Fig. S10, Supplemental Tables S2 and S5). Among these, 6 genes are highly expressed specifically in the AZ. Expression of the endoglucanase gene *Et_8B_060836* in the AZ at s3 is 93 times the average expression level of all GH9 endoglucanase genes across all developmental stages and tissue types. Similarly, expression of xylanase homoeologs *Et_3A_026233* and *Et_3B_030613*, pectate lyase homoeologs *Et_2A_016561* and *Et_2B_020615*, and PME *Et_1B_011134* in the AZ at s3 are 55, 45, 176, 118, and 122 times the average expression within their classes of enzymes, respectively. In addition, GH5 enzyme *Et_4B_038391* (annotated as mannanase) and PAE *Et_1B_011630* have the highest expression among the same class of enzymes in the AZ at s3. In contrast, although XTH *Et_4B_039799*, expansin *Et_4B_037842*, and PMEI *Et_1B_012842* are enriched in the AZ, their absolute expression level is relatively low, and thus, they may be less important in cell wall modification during abscission (Supplemental Fig. S10, Supplemental Table S5).

We tested for changes in cell wall components during development using antibodies including Carbohydrate-Binding Module 3a (CBM3a) targeting cellulose, LM11 preferentially targeting xylan, LM19 preferentially targeting unesterified homogalacturonan (HG), and LM20 preferentially targeting esterified HG. We focused on the AZ region including the stalk and the green tissue immediately below the caryopsis at s2 and s3 before and after abscission (Fig. 8). Cell wall composition is not uniform in the region of interest, so photos of longitudinal sections were manually marked as AZ-stalk, AZ-seed, and green tissue on the palea side and on the lemma side. All 4 antibodies differed significantly among these regions (2-way ANOVA, $P < 0.05$; Supplemental Table S1,

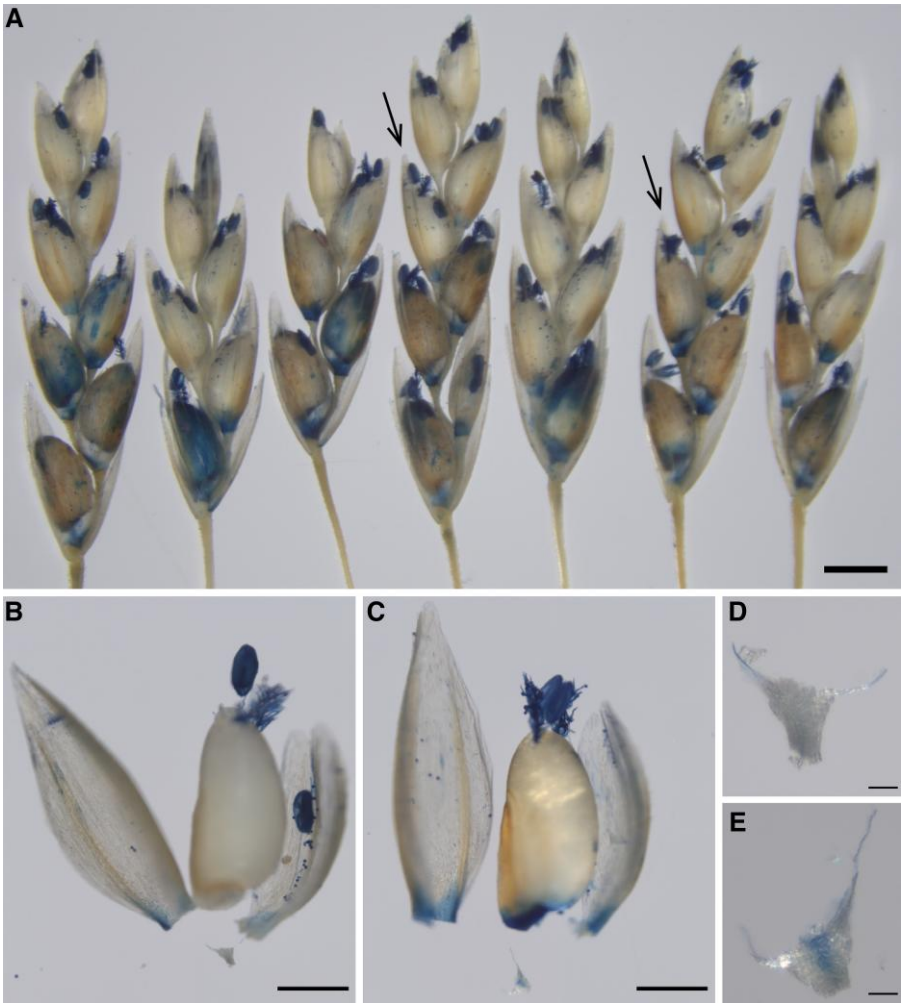

Figure 5 Trypan blue staining shows cell death in the caryopsis AZ of *E. tef*. (A) Examples of *E. tef* spikelets stained with Trypan blue. Scale bar = 1 mm. (B, C) Dissected florets indicated by arrows on the left and the right from (A), respectively. Scale bars = 500 μm. (D, E) Enlarged images of the triangle stalks from (B) and (C), respectively. Scale bars = 50 μm.

Fig. 8). Only LM19 differed significantly among developmental stages, with a stronger signal in all regions at the stage when the caryopsis has detached from the stalk (Tukey's test; $P = 0.003$ between s3 detached and s2, and $P = 0.0007$ between s3 detached and s3 attached). The LM19 signal is much stronger than LM20, indicating that unesterified HG is much more abundant than esterified HG (Fig. 8M–Y). Overall, these results indicate modification of pectin during maturation but no clear evidence of cell wall degradation.

YAB2-LIKE1 (*YAB2L1*) is a hub gene of the AZ module at the early seed maturity stage

Next, we tested if any of the known AZ genes are enriched in the AZ of *E. tef*. We identified the putative *E. tef* orthologs of the known shattering genes in the grass family and analyzed their expression patterns. All tested genes are expressed in at least 1 tissue type and developmental stage, with homoeologs often having similar but not identical expression patterns. One homoeolog of *YAB2/SH1* belongs to AZ module grey60 as does 1 of *qSH1*, and 1 *LES1* homoeolog belongs to AZ module violet, but expression of these genes is not significantly enriched in the AZ. In addition, both copies of *SHAT1* are significantly enriched in the AZ at s3 and belong to AZ module blue (Fig. 9A, Supplemental Tables S2 and S5).

We tested whether other YABBY genes are enriched in the AZ of *E. tef*. In addition to *YAB2/SH1*, 13 *YABBY* genes were expressed in our RNA-Seq data. Both copies of *YAB2-LIKE1* (*YAB2L1*), which share the highest similarities with *YAB2/SH1* (65% between *Et_10A_000629* and both homoeologs of *YAB2/SH1*, and 73% between *Et_10B_002778* and *YAB2/SH1*), are statistically enriched in the AZ at s2 and s3 and belong to the blue AZ module. Both homoeologs of *CRABS CLAW* (*CRC*)*-like* genes have higher expression in the AZ at s3, although only 1 copy is significantly enriched (Fig. 9A). Additionally, 1 *EtYABL1* homoeolog (*Et_10A_000629*) is a hub gene of module blue. Among the genes with the highest

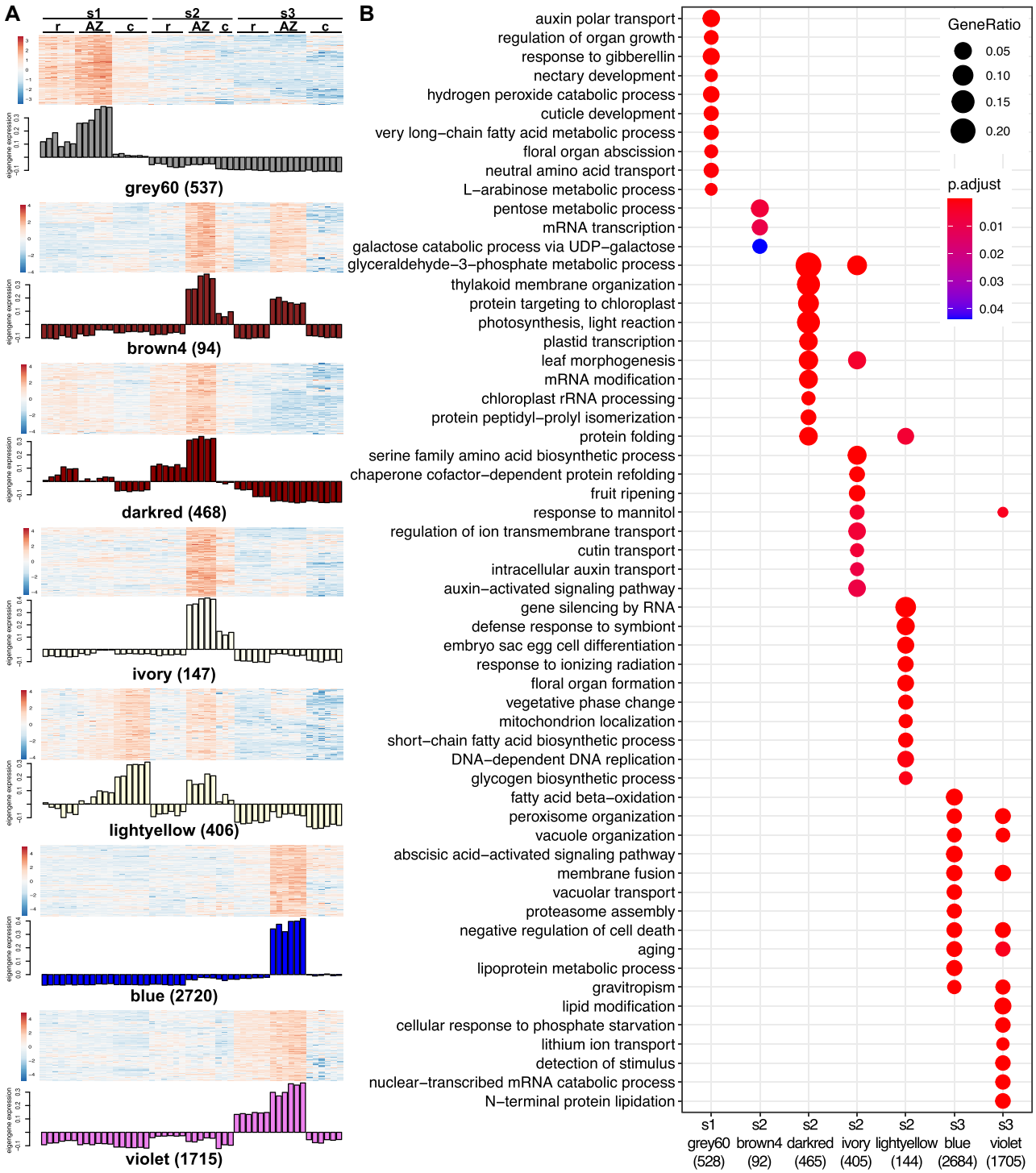

Figure 6 Different functional categories are enriched in AZ expression modules. (A) Heatmap and eigengene expression showing gene modules that are enriched in the AZ at different developmental stages. s1, before anthesis; s2, seed filling; s3, early seed maturity stage. c, caryopsis; r, rachilla. Numbers in parentheses are the number of genes in each module. (B) Top 10 most significant GO terms enriched in each AZ module. Red and blue represent smaller and larger *P*-values, respectively. The size of the dots represents the ratio of genes in each GO term over the total number of genes in the AZ module. Numbers in parentheses are the numbers of genes that are annotated with a GO term in each module.

5% interaction weight with *EtYABL1*, we found genes related to cell death and protein degradation including *Autophagy*, *Clp ATPase*, *AAA ATPase*, *F-box*, and *E3 ubiquitin ligase*, and genes related to cell wall degradation including *Mannanase*, *Pectate lyase*, and *Xylanase* (Fig. 9B, Supplemental Table S6).

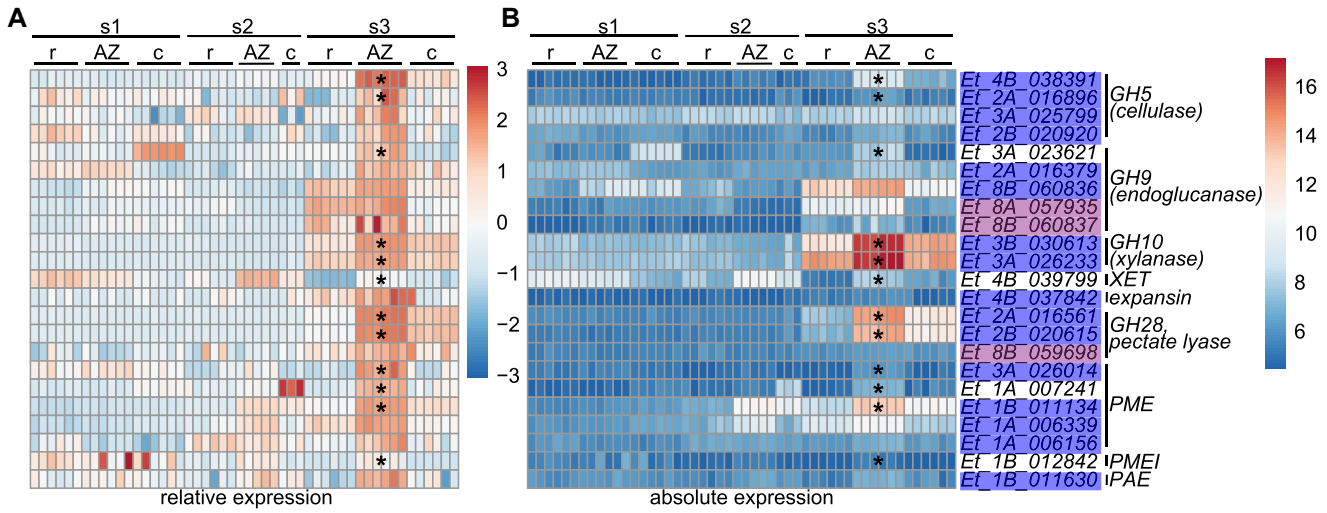

Figure 7 Cell wall-modifying enzymes are enriched in the AZ at the early seed maturity stage. (A) Heatmap of relative expression normalized by each gene. (B) Heatmap of absolute expression of each gene. s1, before anthesis; s2, seed filling; s3, early seed maturity stage. Stars denote significant enrichment by at least 2-fold in the AZ compared with the rachilla and caryopsis (Wald test, adjusted $P < 0.05$). Blue or purple shading on gene names indicates AZ modules as defined by WGCNA. c, caryopsis; r, rachilla.

Discussion

Abscission of *E. tef* occurs through physical rupture rather than cell separation

Current abscission models suggest that abscission occurs through the degradation of the middle lamella and shared wall between cells, resulting in cell separation. After abscission, a smooth fracture plane is often observed and a protective layer immediately proximal to the AZ is differentiated (Patterson 2001; Roberts et al. 2002). In the Arabidopsis floral AZ, the cells remaining on the receptacle elongate after abscission and a layer of cutin accumulates on the outside of the cell wall, while lignin is formed in the cells of the shedding floral organs, preventing the wall hydrolyzing enzymes from diffusing out of the AZ (Lee et al. 2018). Additionally, suberin may also be deposited to protect the exposed cells after abscission (Roberts et al. 2000). In grasses, the presence of a smooth fracture surface is often used as an indicator of easy shattering, such as in African wild rice (*Oryza barthii*) (Lv et al. 2018), *S. viridis* (Hodge and Kellogg 2016), and Siberian wild rye (*Elymus sibiricus* L.) (Zhao et al. 2017). However, such precise cell separation is not required for abscission of *E. tef*, as a rough fracture surface and open cells on the caryopsis side were observed after abscission (Figs. 3 and 4C, Supplemental Fig. S4, F–H). Multiple layers of collapsed pericarp (ovary wall) cells remain between the embryo and the AZ fracture surface, and could serve to protect the embryo (Fig. 2D and 3H, Supplemental Figs. S3 and S6, F–H). In Arabidopsis silique dehiscence, cell rupture occurs in addition to cell separation, suggesting both mechanisms could contribute to abscission simultaneously (Ogawa et al. 2009).

Cell walls may be modified in abscission of *E. tef*

In *E. tef*, the cell walls in the AZ are thin and non-lignified (Fig. 4, Supplemental Fig. S4), and the AZ is only a few cell layers wide (Fig. 3, G and H, Supplemental Fig. S3), forming a natural weak spot for the mature seed to break off even without cell wall breakdown. Nonetheless, our RNA-Seq data showed that genes encoding endo-1,4-β-glucanase, xylanase, pectate lyase, and PME are highly upregulated in the AZ before abscission (Fig. 7, Supplemental Fig. S10, Supplemental Table S5), suggesting that cell walls may break down in these cells. Although these enzymes are all encoded by large gene families, only a couple of genes (often pairs of homoeologs) are highly expressed in a temporally and spatially specific manner, suggesting that they may play specific roles in cell wall degradation and modification that may facilitate abscission.

Conversely, our immunofluorescence data only partially support cell wall modification in the AZ during abscission. The signal of LM19 which preferentially labels unesterified HG is significantly higher in the AZ and surrounding cells detached from the stalk compared with the AZ at earlier stages (Fig. 8, P–R and Y). An increase in unesterified HG was also observed in the AZ of oil palm fruit right before and after abscission induced by ethylene, assayed by immunofluorescence with JIM5, an antibody similar to LM19 (Roongsattham et al. 2016). An increase in unesterified HG may result from the activity of PME that removes the methyl groups of esterified HG. De-esterified HG may be further depolymerized by PG or crosslinked with calcium to form a rigid cell wall (Daher and Braybrook 2015). The former promotes cell separation through the middle lamella, and the latter may promote cell fracture, although additional studies would be required to demonstrate which is the case for *E. tef* AZ.

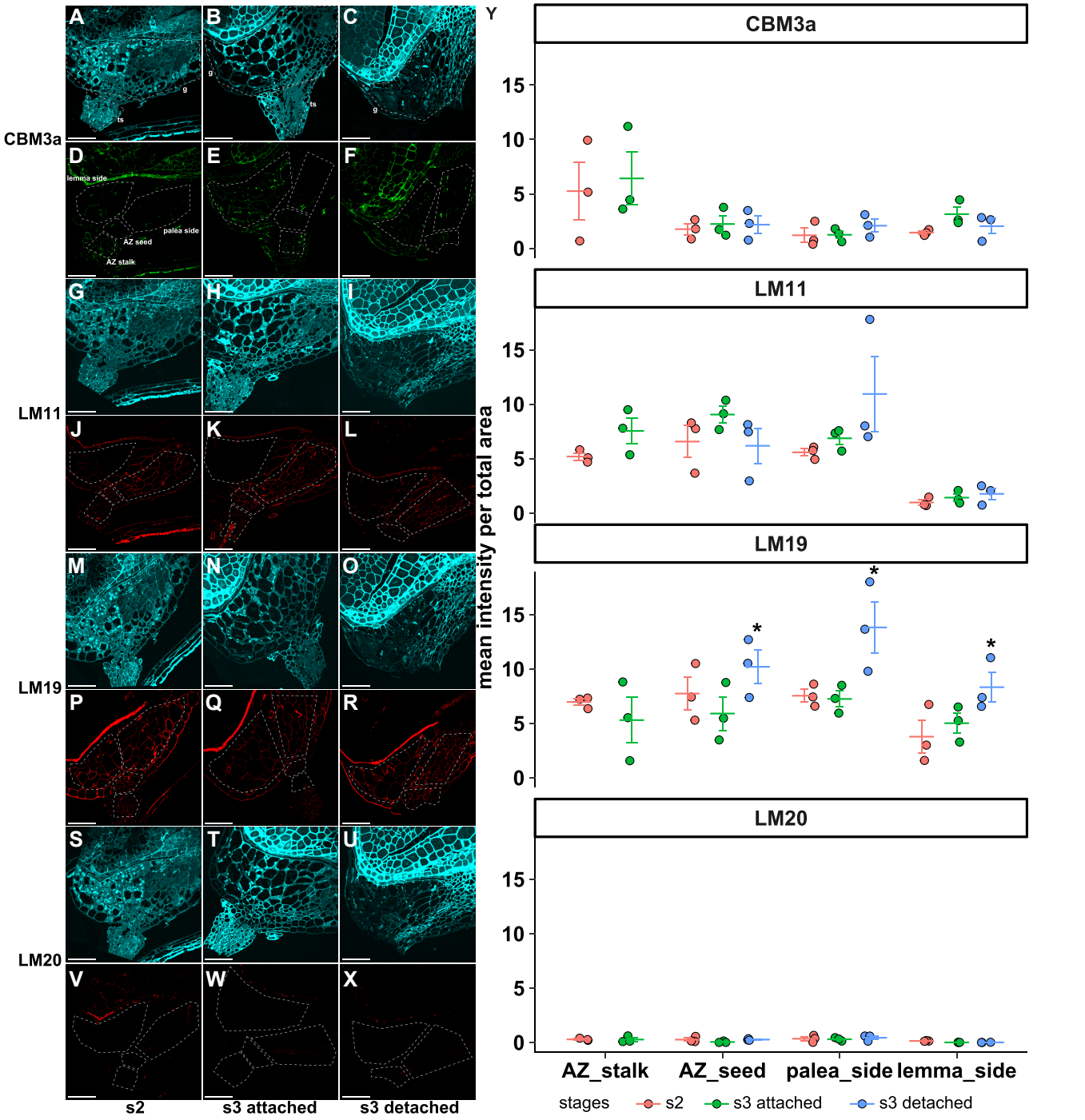

Figure 8 Some cell wall components differ among developmental stages. (A–X) Representative images of immunofluorescence with antibodies (A–F) CBM3a, (G–L) LM11, (M–R) LM19, and (S–X) LM20. (A–C, G–I, M–O, S–U) Autofluorescence. (D–F, J–L, P–R, V–X) Antibody signals. Different sections from the same samples were used for different antibody labeling. The AZ and its surrounding tissues are manually divided into AZ-stalk, AZ-seed, photosynthetic ovary wall on the palea side, and the lemma side. Images are enhanced for visualization, and raw images were used for quantification. Scale bars = 50 μm. (Y) Signal intensity of the 3 biological replicates (circles) and mean ± standard error (lines) within each region for each antibody. Stars denote significant differences (Tukey's test, $P < 0.01$) between developmental stages. S2, seed filling stage; s3-attached, early seed maturity stage before abscission; s3-detached, post-abscission stage. g, green tissue at the bottom of the caryopsis; ts: triangular stalk.

We did not observe differences in cellulose labeled with CMB3a, xylan labeled with LM11, and esterified HG labeled with LM20 (Fig. 8). This may indicate a lack of modification of these wall components, but may also indicate that our antibodies are not sensitive enough; cell wall components are complex and the antibodies often only label a specific

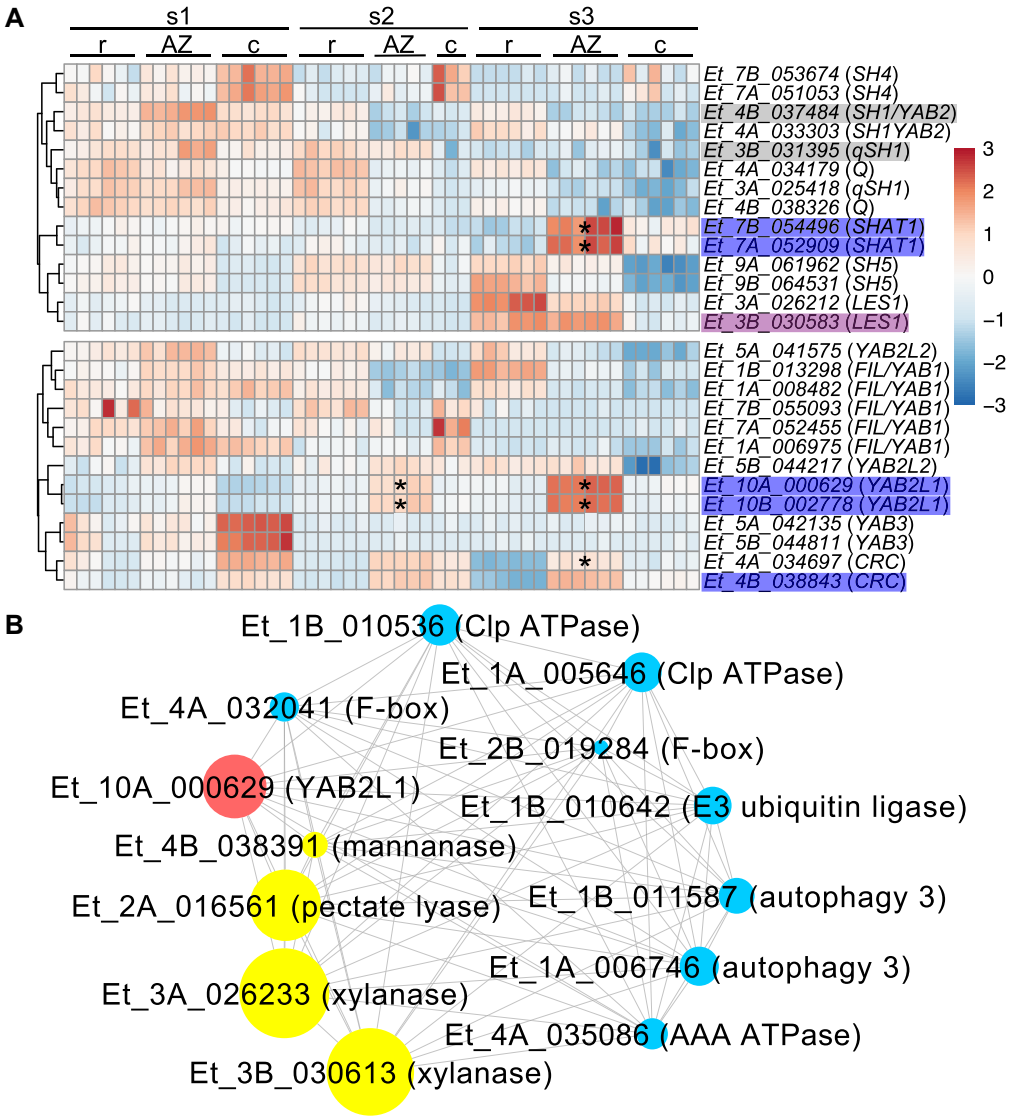

Figure 9 Putative orthologs of previously identified AZ genes are partially enriched in the AZ. (A) Heatmap of relative expression normalized by each gene. s1, before anthesis; s2, seed filling; s3, early seed maturity stage. Stars denote significant enrichment in the AZ by at least 2-fold compared with the rachilla and caryopsis (Wald test, adjusted $P < 0.05$). The gray, blue, or purple shading on gene names indicates the AZ modules defined by WGCNA. c, caryopsis; r, rachilla. (B) Selected *YAB2L1* co-expression network. Genes related to cell wall enzymes (yellow), and protein degradation and cell death (blue) with the top 5% highest weight interaction with *YAB2L1* (red) are shown in the network. The size of the filled circles denotes the absolute expression levels of the genes.

form of the polysaccharides (McCartney et al. 2005). Consistent with this hypothesis, the triple mutant *Arabidopsis dehiscence zone polygalacturonase1 (adpg1) adpg2 quartet2* lacks fruit abscission but has a similar JIM5 signal compared with the wild type (Ogawa et al. 2009).

PCD accompanies abscission in *E. tef*

PCD plays essential roles throughout plant development, including differentiation of xylem tracheids, the tapetum of anthers, maternal tissues during seed development, or senescing organs such as leaf and floral parts (Daneva et al. 2015). PCD may result in degradation (e. g. tapetum cell death and leaf perforation) or preservation (e. g. xylem differentiation) of the cell wall (van Doorn et al. 2011). PCD and abscission both occur in senescing organs. However, direct evidence demonstrating the importance of PCD in abscission is scarce. Suppressing the expression of the S-like RNase *LX* delays both leaf senescence and abscission in tomato, so it is unclear whether delayed abscission is a direct effect of downregulation of *LX* or an indirect effect through delayed senescence (Lers et al. 2006).

In anther dehiscence, PCD occurs in successive layers of cells ending with the stomium, allowing the anther to open and release pollen (Sanders et al. 2005; Senatore et al. 2009; Wilson et al. 2011). Ectopic expression of an aspartic protease in Arabidopsis anther keeps the stomium cells

intact and suppresses dehiscence, although it is unclear whether these cells fail to undergo PCD (Ge et al. 2005).

In seed development of wheat and barley, the pericarp degenerates to provide space and remobilize nutrients to the developing seeds. The dead cells in the pericarp collapse and reduce to several layers of cuticles, serving as a protectant to the embryo (Domínguez and Cejudo 2014; Li et al. 2021). Our results suggest a similar scenario in *E. tef* and probably other *Eragrostis* species. As the caryopsis matures, the cells in the AZ including the photosynthetic ovary wall undergo cell death and collapse, leading to breakage at the weakest cells—the AZ (Figs. 2, C and D, 3, and 5). Since cell death does not occur precisely in the AZ, we infer that PCD accompanies abscission but does not specify the AZ.

Putative YAB2/SH1 paralogs may regulate AZ development of *E. tef*

YAB2/SH1 is so far the only gene that shows conserved roles in abscission across subfamilies of grasses despite their differences in AZ position and anatomy (Lin et al. 2012; Doust et al. 2014; Lv et al. 2018; Odonkor et al. 2018; Yu et al. 2020a, Liu et al. 2022). In *E. tef*, both copies of *YAB2/SH1* are expressed in the AZ, particularly at early developmental stages (Fig. 9A). However, distinct from the knockout studies in rice and *Setaria* (Lv et al. 2018; Liu et al. 2022), the knockout mutants of *EtYAB2/SH1* do not have any shattering phenotype, suggesting that either they do not function in *E. tef* abscission in the caryopsis or lemma, or their function is redundant with other genes (Supplemental Fig. S6). Since most *Eragrostis* species have lost the ancestral AZ position in the rachilla and evolved an AZ position below the caryopsis (Fig. 1) (Yu et al. 2020a), we propose that *YAB2/SH1* may control ancestral AZ development in the grass family, while *Eragrostis* species, including *E. tef*, have evolved a unique mechanism controlling grain shattering through physical fracture. Consistent with this hypothesis, both copies of *YAB2L1* that share the highest similarity with *YAB2/SH1* are highly enriched in the AZ at seed maturation and are co-expressed with cell wall-modifying enzymes and cell death-related genes (Fig. 9, Supplemental Table S6), suggesting that *YAB2L1* could be an upstream regulator of abscission in *E. tef*.

Putative orthologs of known AZ genes in other species are also enriched in the AZ of *E. tef*, including 4 homologs of *BOP2* in the AZ module at s1 (Supplemental Fig. S9A), and both copies of *SHAT1* putative orthologs in the AZ at s3 (Fig. 9A, Supplemental Tables S2 and S5). Both *BOP2* and *SHAT1* define the anatomy of the AZ. In Arabidopsis, *BOP1* and *BOP2* are essential for AZ differentiation. *bop1 bop2* double mutants fail to develop the small and cytoplasmically dense AZ cells at the junction of the receptacle and floral organs as observed in the wild type, and completely abolish floral organ abscission (McKim et al. 2008). In rice, *SHAT1* is strongly and specifically expressed in the AZ. Along with pleiotropic defects in inflorescence development, *shat1* mutants show an extended rachilla at the position of the AZ, and the small AZ cells are replaced by elongated and lignified cells (Zhou et al. 2012). Gene knockouts would be required to validate the role of these genes in *E. tef*.

Loss of lemma shattering may contribute to the domestication of *E. tef*

Although the caryopsis AZ in *E. tef* is similar to that in its wild progenitor *E. pilosa*, the spikelets do shatter less (Phillips 1995), because the tough lemma clasps the caryopsis in the floret (Fig. 2A). Most of the wild *Eragrostis* species studied here have lemmas that break easily, with 1 exception in *E. papposa* (Fig. 1, C–M), suggesting natural variation of lemma toughness in wild *Eragrostis* species. The tough lemma of *E. tef* may have been selected during domestication. Our XRM data and histological staining did not reveal a distinct AZ in the lemma of either *E. pilosa* or *E. tef* (Fig. 2, C–G, Supplemental Fig. S3), so the tough lemma in *E. tef* cannot be due to the loss of a lemma AZ. The main difference between the domesticate and its wild progenitor is that the base of the lemma in the former is much thicker than that of the latter, suggesting that lemma shattering is due to physical fracture and the thicker lemma of *E. tef* is less likely to break off. Future studies are required to test if any physiological process activates lemma shattering in *E. pilosa* but not in *E. tef*. Controlling either caryopsis or lemma shattering will further reduce grain shattering in *E. tef* and increase harvestable yield.

The ancestral AZ is lost in a number of *Eragrostis* species

Our previous study mapped the AZ position of about 250 grass species, including 26 Chloridoideae species, on a grass phylogenetic tree. The ancestral state of the AZ position in the whole grass family and in Chloridoideae is placed in the rachilla below the floret (Yu et al. 2020a). In another study, we compared the AZ anatomy of diverse grass species including 3 Chloridoideae species, *E. tef*, *Sporobolus heterolepis*, and *Bouteloua curtipendula*, and the AZ of *S. heterolepis* is located below the floret (the ancestral position). The AZ of *S. heterolepis* is smaller than the surrounding cells and differentially lignified with upper cells non-lignified and lower cells lignified, resembling a typical AZ anatomy (Roberts et al. 2002; Yu et al. 2020b). The current study sampled 12 *Eragrostis* species, with 7 species abscising only below the caryopsis, 2 species (*E. ciliaris* and *E. tenella*) both below the caryopsis and in the rachilla, and 2 species (*E. lilliputiana* and *E. scabrida*) only in the rachilla (Fig. 1). Histological staining revealed that the rachilla AZ in the 4 *Eragrostis* species is similar to the AZ of *S. heterolepis* in terms of the cell morphology (Supplemental Fig. S2, Yu et al. 2020b). These results suggest that the ancestral rachilla AZ may be lost in the ancestor of *Eragrostis*, while it may have been regained in some species. Alternatively, the *Eragrostis* ancestor may have been polymorphic with both caryopsis and rachilla AZs; in this

scenario, the rachilla AZ would have been lost later on in some species while retained in others. A larger sample size will be required to distinguish these 2 hypotheses.

Materials and methods

Plant materials and growth conditions

Seeds of teff (*E. tef*) (cultivar Dabbi, PI 524438, https://www.ars-grin.gov) were obtained from Dr Robert VanBuren at Michigan State University. Seeds of *E. botryodes* (Ingram 2000-13), *E. ciliaris* (Ingram 605), *E. dielsii* Pilg. (PI 238301), *E. papposa* (Ingram 2000-01), *E. pilgeriana* (Ingram 644), *E. pilosa* (PI 219588), *E. schweinfurthii* (Ingram 2000-12), *E. tenella* (Ingram 606), *E. scabrida* (Columbus 5220), and *E. cyperoides* (Ingram 655) were kindly provided by Dr Amanda L. Ingram at Wabash College. Seeds of *E. lilliputiana* (Columbus 5206) were obtained from Dr. J. Travis Columbus at Claremont Graduate University. *E. scabrida* and *E. lilliputiana* were previously classified as sister genera of *Eragrostis* in tribe Eragrostideae, based on their distinctive morphological traits, but were placed within *Eragrostis* by Barrett et al. (2020).

For experiments involving multiple species comparisons, plants were grown in a greenhouse with 40–50% humidity, 14-h light/10-h dark, and temperatures of 28 °C day/22 °C night. For experiments only on *E. tef*, plants were grown in a growth chamber with 40–60% humidity, 12-h light/12-h dark, and temperatures of 31 °C day/22 °C night.

Histology and light microscopy

Histological experiments followed standard procedures as described previously (Yu et al. 2020b) and in Supplemental Methods S1.

X-ray microscopy

Sample preparation and XRM imaging methods were adapted from Duncan et al. (2022). A combination fixation-contrast solution, ethanolic phosphotungstic acid (ePTA), was prepared at 1% PTA (w/v) in 70% ethanol (v/v). Live *E. tef* spikelets were transferred to 10 mL of ePTA in 20 mL glass sample vials and placed on a lab rocker at room temperature (RT) for at least 21 d before imaging, and the ePTA solution was exchanged at 7 and 14 d. For XRM imaging, a single fixed and contrast-enhanced spikelet was rinsed for 10 min in distilled water, then transferred to a 0.2 mL flat-cap PCR tube filled with melted low melting point agarose at 2% (w/v) in distilled water. When the agarose had solidified, the sample tube was mounted on the end of a wooden applicator stick using a 2-stage 5-min epoxy resin and placed in the XRM sample holder. Imaging was done on a ZEISS Xradia 520 Versa X-ray microscope using a 20× objective lens with the following instrument settings: 60 kV, 5 W, 83 μA, binning = 2, exposure = 7 s, 4,001 projections, geometric magnification = 1.8× for a voxel resolution of 0.7 μm. Scans were automatically reconstructed using ZEISS Reconstructor software, and image analysis used ORS Dragonfly for noncommercial users. Lemma width was estimated using the formula area/perimeter*2 measured by Dragonfly software (Object Research Systems, Montréal, Canada).

Scanning electron microscopy

Caryopses before and after abscission were dissected and fixed in 2% (w/v) paraformaldehyde and 2% (w/v) glutaraldehyde with 0.1% (v/v) Tween20 in 0.1 M cacodylate buffer at pH 7.4, vacuum infiltrated for 10 min, kept at RT for 2 h, followed by overnight incubation at 4 °C. After 3 rinses in 0.1 M cacodylate buffer for 15 min each, tissues were post-fixed in 1% (w/v) osmium tetroxide in cacodylate buffer for another 3 h, followed by 3 rinses in water. Then samples were placed in 1% (w/v) aqueous uranyl acetate at 4 °C overnight, then 50 °C for 2 h, followed by another 3 rinses in water.

The samples were then dehydrated in an ethanol series, critical point dried in a Tousimis Samdri-780A critical point dryer, mounted on aluminum stubs with double-stick carbon adhesive tabs, Au/Pd coated in a Tousimis Samsputter-2a. Images were digitally acquired at 1280×960 pixel resolution at 20 kV, a current of 6.6 μA, magnification of 100× and 1500× at a working distance of 12.6 to 12.8 mm on a Hitachi S-2600H SEM.

Transmission electron microscopy

Florets at pre-anthesis (s1), seed filling (s2), and maturation (s3) stages were dissected and fixed as in the SEM procedure. After fixation and post-fixation steps, samples were dehydrated in a graded acetone series (30%, 50%, 70%, 80%, 90%, 100%, 100%, 100% v/v) for 15 to 30 min each. Then tissues were infiltrated in a series of Quetol 651 epoxy resin (20%, 40%, 60%, 80%, 100%, 100% v/v) for 12 to 24 h with acetone as solvent and polymerized in Quetol 651 resin at 60 °C for 48 h. Specimens were then sectioned at 60 nm using a Leica Ultracut UCT ultramicrotome, mounted on 200 mesh formvar/carbon-coated copper grids, stained with lead citrate for 8 min, and imaged using a LEO 912 AB Energy Filter Transmission Electron Microscope (Zeiss, Oberkochen, Germany). Images were acquired with iTEM software (ver. 5.2) (Olympus Soft Imaging Solutions GmbH, Münster, Germany) with a TRS 2048 × 2048k slow-scan charge-coupled device camera (TRÖNDLE Restlichtverstärkersysteme, Moorenweis, Germany). About 3 to 4 biological samples per stage were observed.

Trypan blue staining

Spikelets were dissected and immersed in commercial 0.4% (w/v) trypan blue solution (G-Biosciences) for 1 h at RT. Samples were incubated in 100% ethanol overnight to remove chlorophyll and kept in 100% ethanol in a petri dish for imaging with a ZEISS Axio Zoom.V16 Fluorescence Stereo Zoom Microscope. Z-stack images were processed using the Extended-Depth-of-Focus function in ZEISS Zen Blue software (Version 2.3).

Generation of *Etyab2* CRISPR mutants in *E. tef*

gRNAs were designed to target *EtYAB2* in both subgenomes using the online tool CRISPOR (Concordet and Haeussler 2018). Two gRNAs targeting TAGCAAACATGCTCCG GCGC and AACATCGTGACTGTCCGTTG were selected and cloned into module B vector pMOD_B2518 with restriction enzyme BsmBI, and module C vector pMOD_C2616 with BsaI, respectively, using GoldenGate cloning system. Module A vector pMOD_A1110 carrying the *ZmUbi1promoter:TaCas9* was then assembled with modules B and C vectors into the destination vector pTRANS_250d using AarI enzyme (Čermák et al. 2017). Then the sequences including *ZmUbi1promoter:TaCas9* and the 2 gRNAs were PCR amplified using primers Infu78891 FP and Infu78891 RP (Supplemental Table S7) and cloned into the PHP78891 vector via FseI restriction sites using infusion cloning (TaKaRa Bio, Kusatsu, Shiga, Japan). PHP78891 harbors *BABY BOOM*, *WUSCHEL* (Lowe et al. 2016), and a desiccation inducible RAB17M promoter-driven *CRE* gene, which induces cleavage of the transgenes inside the loxP sites (Mookkan et al. 2017). Transformation and regeneration of transgenic lines were carried out as described by Beyene et al. (2022) and in Supplemental Methods S1.

RNA-Seq library preparation

Florets at s1, s2, and s3 were dissected and tissues surrounding the AZ, immediately above (the lower part of caryopsis), and below (the rachilla) were collected using a scalpel under a dissecting microscope (Supplemental Fig. S8), and stored in 2 mL tubes surrounded by liquid nitrogen. Around 80 to 100 dissected tissues were pooled for each biological sample and 6 biological replicates were collected. Dissected tissues were ground, and total RNA was isolated using a PicoPure RNA Isolation Kit with in-column DNase I treatment following the manufacturer's instructions. 3′ mRNA-Seq libraries were constructed using QuantSeq 3′ mRNA-Seq Library Prep Kit FWD for Illumina (Lexogen, Vienna, Austria) (Moll et al. 2014). In total, 50 libraries were successfully constructed (4 samples failed to amplify for unknown reasons) and were subjected to single-end sequencing at 100 nt on an Illumina NovaSeq platform with S prime flow cells at the Roy J. Carver Biotechnology Center at the University of Illinois at Urbana-Champaign. Sequences have been deposited in the Sequence Read Archive (BioProject ID PRJNA885107).

RNA-Seq analysis

Sequences were trimmed using cutadapt 3.2 (Martin 2011) and mapped to the *E. tef* v3 genome (CoGe id50954) (VanBuren et al. 2020) using STAR software (v2.7.8a) (Dobin et al. 2013). Because 3′ UTRs were not annotated, 500 bp were extended to each gene model at the 3′ end to increase the mapping rate. Mapped read counts were calculated using htseq-count (HTSeq v0.11.4) (Anders et al. 2015). Raw counts were then input into DESeq2 (v1.22.2) in R (v3.5.0) (Love et al. 2014), and genes with less than 10 normalized average counts at each condition were removed because of low expression before gene differential expression and co-expression analyses. Two-fold change and adjusted *P*-values lower than 0.05 were used as thresholds for significant differential gene expression.

Gene co-expression networks were constructed in WGCNA (v1.66), using normalized counts with soft-thresholding power of 9, minimal module size of 60 genes, cutHeight of 0.1, and deepSplit of 2 (Langfelder and Horvath 2008). Hub genes within each module were identified using intramodular connectivity and signed eigengene-based connectivity implemented in WGCNA. The 10% of genes with the highest connectivity in both methods were treated as hub genes in a module. Co-expressed genes of *YAB2L1* were defined as genes in the top 5% highest weight of interaction with *YAB2L1* and were visualized using CytoScape v3.8.2 (Shannon et al. 2003). Gene names and categorization were manually curated based on the annotation of their putative rice orthologs identified by OrthoFinder (Emms and Kelly 2015). R scripts for the analyses are available at https://github.com/Yunqing-Yu/tef-abscission-zone.

GO enrichment analysis

GO terms of *E. tef* v3 protein sequences were annotated using the Gene Ontology Meta Annotator for Plants (GOMAP) pipeline (Wimalanathan and Lawrence-Dill 2021). In total, 67,018 of 68,255 (98.2%) sequences were successfully annotated, and the median number of annotated GO terms per gene was 8. Functional annotation of genes was based on their putative rice orthologs. The *E. tef* organism GO annotation database was built using the function "makeOrgPackage" in the package of AnnotationForge in R. GO enrichment analysis of genes enriched in the AZ was performed using the clusterProfiler package in R with default settings except that biological process was used for the sub-ontology type, and maximum set as 1,000 (Yu et al. 2012). Redundant terms were identified and removed using the "simplify" function implemented in clusterProfiler with a cut-off of 0.6 and measure of "Rel," plus manual curation.

Identification of putative cell wall-related enzymes

Cell wall-modifying enzymes of interest were identified through Pfam domain search. Relevant enzyme families include glycosyl hydrolase family 5 (PF00150) which has cellulase activity, glycosyl hydrolase family 9 (PF00759) which has endoglucanase activity, glycosyl hydrolase family 10 (PF00331) which has xylanase activity, xyloglucan endo-transglycosylase (XET) C-terminus (PF06955), glycosyl hydrolases family 28 (PF00295) which has polygalacturonase and rhamnogalacturonase A activity, pectate lyase superfamily (PF12708 and PF00544), expansion C-terminal domain (PF01357), pectinacetylesterase (PF03283), pectinesterase (PF01095), and plant invertase/pectin methylesterase inhibitor (PF04043). Raw HMM files of these enzymes were downloaded from https://www.ebi.ac.uk/interpro/, and used for

searching against the annotated proteins from the *E. tef* v3 genome using hmmsearch with a sequence reporting threshold of 0.01 and domain reporting threshold of 0.1 (HMMER 3.1b2; http://hmmer.org/). These protein sequences were then used as queries to identify the Arabidopsis homologs using blastp with default settings. If the Arabidopsis homologs were not annotated as the expected enzymes on The Arabidopsis Information Resource (TAIR), then these proteins were excluded from downstream analyses.

Immunofluorescence

Caryopses at s2 and s3 before and after abscission were dissected and fixed in 4% paraformaldehyde (w/v) and 0.5% (w/v) glutaraldehyde with 0.1% (v/v) Tween20 in 0.1 M PIPES buffer at pH 7.4, vacuum infiltrated for 10 min, kept at RT for 2 h, followed by overnight incubation at 4 °C. Samples were dehydrated with an ethanol series, infiltrated with Lowicryl HM20 resin (Electron Microscopy Sciences, Hatfield, USA), and polymerized in an EMS UVC3 Ultraviolet Cryo Chamber (Electron Microscopy Science). Specimens were sliced into 250 nm thin sections using a Leica Ultracut UCT ultramicrotome and dried onto a silanized coverslip. For immunofluorescence, sections were treated with fresh 0.1% (w/v) sodium borohydride in 1× PBS buffer for 30 min to quench autofluorescence, rinsed in 1× PBS buffer 3 times for 5 min each, then treated with 0.05 M glycine in 1× PBS buffer for 15 min to inactivate residual aldehyde groups. Samples were then incubated in blocking buffer (5% (w/v) BSA in 1× PBST, 0.5% (v/v) Tween-20) for 1 h. Rat primary antibodies (LM11, LM19, and LM20) were diluted in blocking buffer with a ratio of 1:15 and 1:100 for CBM3a (PlantProbes, https://plantcellwalls.leeds.ac.uk/science/antibodies/) and applied to the samples for 1 h at RT. Samples were rinsed in blocking buffer 3 times for 10 min each, then incubated with Alexa Fluor 594 goat anti-rat secondary antibody (Thermo Fisher Scientific, Waltham, USA) diluted 300× in blocking buffer for LM11, LM19, and LM20. For CBM3a, samples were incubated with a secondary antibody 6x-His Tag Monoclonal Antibody (HIS.H8, Thermo Fisher Scientific) diluted 500 times for 1 h at RT, followed by incubating with a tertiary antibody Alexa Fluor 488 goat anti-mouse antibody diluted 500 times overnight at 4 °C. Samples were then washed with 1× PBST twice for 15 min each and stored in 1× PBS at 4 °C before imaging. The fluorescence signal was imaged with a TCS SP8-X confocal microscope (Leica Microsystems, Wetzlar, Germany) with an HC PL APO CS2 63×/1.20 water objective lens. The detailed imaging setting was described in Supplemental Methods S1.

Accession numbers

Sequence data used in this article can be found in the CoGe data libraries under accession number CoGe id50954. RNA-Seq data from this article can be found in Sequence Read Archive under BioProject ID PRJNA885107.

Acknowledgments

We thank Dr Robert VanBuren at Michigan State University for providing seeds of *E. tef*, Drs Amanda L. Ingram at Wabash College and J. Travis Columbus at Claremont Graduate University for seeds of wild *Eragrostis* species. We thank Dr Sébastien Bélanger at the Donald Danforth Plant Science Center (DDPSC) for the help on YAB2 sequence analysis. We thank Corteva Agriscience for providing binary vector PHP78891 and *A. tumefaciens* strain LBA4404 THY. We acknowledge imaging support from the Advanced Bioimaging Laboratory (RRID:SCR_018951) at DDPSC and usage of the LEO 912AB Energy Filter TEM acquired through an NSF DBI-0116650. The X-ray microscope is part of Dr Chris Topp's lab under a research collaboration with Sumitomo Chemical Company, Valent BioSciences, and DDPSC.

Author contributions

The project was designed by Y.Y., G.B., N.J.T., and E.A.K. Y.Y. did all microscopy, immunolocalization, phylogenetic analysis, and molecular cloning and generated all RNA-seq data. A.N.D., H.H., and Y.Y. analyzed the RNA-Seq data. G.B., J.V., and N.J.T. did plant transformations. K.E.D. provided XRM data. Y.Y. and T.J. phenotyped and genotyped transgenics. A.N.D., G.B., E.A.K., and N.J.T. secured funding. Y.Y. drafted the manuscript and figures. All authors edited the manuscript and approved the contents.

Supplemental data

The following materials are available in the online version of this article.

Supplemental Table S1. Results of 2-way ANOVA analyses.

Supplemental Table S2. Genes in the AZ modules from WGCNA.

Supplemental Table S3. GO enrichment analysis of the AZ modules.

Supplemental Table S4. Hub genes of the AZ modules.

Supplemental Table S5. Differential gene expression analysis by DESeq2.

Supplemental Table S6. YAB2L1 co-expressed genes with the 5% highest interaction weight.

Supplemental Table S7. Primers used for genotyping *Etyab2* mutants.

Supplemental Methods S1. Supplemental materials and methods.

Supplemental Figure S1. The bottom of the caryopsis is photosynthetic in *Eragrostis* species.

Supplemental Figure S2. The rachilla AZ in *Eragrostis* species has typical AZ anatomy.

Supplemental Figure S3. The lemma of *E. tef* is thicker than that of *E. pilosa*.

Supplemental Figure S4. Cell wall breakage is observed in the AZ cells at the early seed maturity stage.

Supplemental Figure S5. CRISPR-Cas9 gene editing results in insertions in the guide RNA-targeted regions.

Supplemental Figure S6. The *yab2* mutants have the same phenotypes as the wild type (wt).

Supplemental Figure S7. Single nucleotide polymorphisms in *EtYAB2/SH1* compared with other YAB2 sequences.

Supplemental Figure S8. Representative images of samples used for RNA-Seq analysis.

Supplemental Figure S9. Heatmap of selected genes in the AZ modules.

Supplemental Figure S10. Heatmaps of cell wall-modifying enzymes.

Funding

This project is supported by NSF-IOS 1938086 to E.A.K., NSF-IOS 1938093 to A.D., and a grant from the Enterprise Rent-a-Car foundation at DDPSC to Y.Y., G.B., E.A.K., and N.T.

Conflict of interest statement. The authors declare no conflict of interest.

References

Anders S, Pyl PT, Huber W. HTSeq—a Python framework to work with high-throughput sequencing data. Bioinformatics. 2015:**31**(2):166–169. https://doi.org/10.1093/bioinformatics/btu638

Bar-Dror T, Dermastia M, Kladnik A, Znidaric MT, Novak MP, Meir S, Burd S, Philosoph-Hadas S, Ori N, Sonego L, et al. Programmed cell death occurs asymmetrically during abscission in tomato. Plant Cell. 2011:**23**(11):4146–4163. https://doi.org/10.1105/tpc.111.092494

Barrett RL, Peterson PM, Romaschenko K. A molecular phylogeny of *Eragrostis* (Poaceae: Chloridoideae: Eragrostideae): making lovegrass monophyletic in Australia. Aust Syst Bot. 2020:**33**(5):458–476. https://doi.org/10.1071/SB19034

Beyene G, Chauhan RD, Villmer J, Husic N, Wang N, Gebre E, Girma D, Chanyalew S, Assefa K, Tabor G, et al. CRISPR/Cas9-mediated tetra-allelic mutation of the "Green Revolution" *SEMIDWARF-1* (*SD-1*) gene confers lodging resistance in Tef (*Eragrostis tef*). Plant Biotechnol J. 2022:**20**(9):1716–1729. https://doi.org/10.1111/pbi.13842

Bowman JL. The YABBY gene family and abaxial cell fate. Curr Opin Plant Biol. 2000:**3**(1):17–22. https://doi.org/10.1016/S1369-5266(99)00035-7

Brummell DA, Hall BD, Bennett AB. Antisense suppression of tomato endo-1,4-β-glucanase *Cel2* mRNA accumulation increases the force required to break fruit abscission zones but does not affect fruit softening. Plant Mol Biol. 1999:**40**(4):615–622. https://doi.org/10.1023/A:1006269031452

Čermák T, Curtin SJ, Gil-Humanes J, Čegan R, Kono TJY, Konečná E, Belanto JJ, Starker CG, Mathre JW, Greenstein RL, et al. A multipurpose toolkit to enable advanced genome engineering in plants. Plant Cell. 2017:**29**(6):1196–1217. https://doi.org/10.1105/tpc.16.00922

Chanyalew S, Ferede S, Damte T, Fikre T, Genet Y, Kebede W, Tolossa K, Tadele Z, Assefa K. Significance and prospects of an orphan crop tef. Planta. 2019:**250**(3):753–767. https://doi.org/10.1007/s00425-019-03209-z

Cho H-T, Cosgrove DJ. Altered expression of expansin modulates leaf growth and pedicel abscission in *Arabidopsis thaliana*. Proc National Acad Sci. 2000:**97**(17):9783–9788. https://doi.org/10.1073/pnas.160276997

Concordet J-P, Haeussler M. CRISPOR: intuitive guide selection for CRISPR/Cas9 genome editing experiments and screens. Nucleic Acids Res. 2018:**46**(W1):W242–W245. https://doi.org/10.1093/nar/gky354

Daher FB, Braybrook SA. How to let go: pectin and plant cell adhesion. Front Plant Sci. 2015:**6**:523. https://doi.org/10.3389/fpls.2015.00523

Daneva A, Gao Z, Durme MV, Nowack MK. Functions and regulation of programmed cell death in plant development. Annu Rev Cell Dev Bi. 2015:**32**:1–28. https://doi.org/10.1146/annurev-cellbio-111315-124915

del Campillo E, Bennett AB. Pedicel breakstrength and cellulase gene expression during tomato flower abscission. Plant Physiol. 1996:**111**(3):813–820. https://doi.org/10.1104/pp.111.3.813

Dobin A, Davis CA, Schlesinger F, Drenkow J, Zaleski C, Jha S, Batut P, Chaisson M, Gingeras TR. STAR: ultrafast universal RNA-seq aligner. Bioinform Oxf Engl. 2013:**29**(1):15–21. https://doi.org/10.1093/bioinformatics/bts635

Domínguez F, Cejudo FJ. Programmed cell death (PCD): an essential process of cereal seed development and germination. Front Plant Sci. 2014:**5**:366. https://doi.org/10.3389/fpls.2014.00366

Dong Y, Wang Y-Z. Seed shattering: from models to crops. Front Plant Sci. 2015:**6**:476. https://doi.org/10.3389/fpls.2015.00476

Doust AN, Lukens L, Olsen KM, Mauro-Herrera M, Meyer A, Rogers K. Beyond the single gene: how epistasis and gene-by-environment effects influence crop domestication. Proc National Acad Sci. 2014:**111**(17):6178–6183. https://doi.org/10.1073/pnas.1308940110

Duncan KE, Czymmek KJ, Jiang N, Thies AC, Topp CN. X-ray microscopy enables multiscale high-resolution 3D imaging of plant cells, tissues, and organs. Plant Physiol. 2022:**188**(2):831–845. https://doi.org/10.1093/plphys/kiab405

Emms DM, Kelly S. Orthofinder: solving fundamental biases in whole genome comparisons dramatically improves orthogroup inference accuracy. Genome Biol. 2015:**16**(1):157. https://doi.org/10.1186/s13059-015-0721-2

Ge X, Dietrich C, Matsuno M, Li G, Berg H, Xia Y. An *Arabidopsis* aspartic protease functions as an anti-cell-death component in reproduction and embryogenesis. Embo Rep. 2005:**6**(3):282–288. https://doi.org/10.1038/sj.embor.7400357

Gonzalez-Bosch C, del Campillo E, Bennett AB. Immunodetection and characterization of tomato endo-β-1,4-glucanase Cel1 protein in flower abscission zones. Plant Physiol. 1997:**114**(4):1541–1546. https://doi.org/10.1104/pp.114.4.1541

González-Carranza ZH, Elliott KA, Roberts JA. Expression of polygalacturonases and evidence to support their role during cell separation processes in *Arabidopsis thaliana*. J Exp Bot. 2007:**58**(13):3719–3730. https://doi.org/10.1093/jxb/erm222

González-Carranza ZH, Whitelaw CA, Swarup R, Roberts JA. Temporal and spatial expression of a polygalacturonase during leaf and flower abscission in oilseed rape and Arabidopsis. Plant Physiol. 2002:**128**(2):534–543. https://doi.org/10.1104/pp.010610

Hodge JG, Kellogg EA. Abscission zone development in *Setaria viridis* and its domesticated relative, *Setaria italica*. Am J Bot. 2016:**103**(6):998–1005. https://doi.org/10.3732/ajb.1500499

Ingram AL, Doyle JJ. The origin and evolution of *Eragrostis tef* (Poaceae) and related polyploids: evidence from nuclear *waxy* and plastid *rps16*. Am J Bot. 2003:**90**(1):116–122. https://doi.org/10.3732/ajb.90.1.116

Jiang C-Z, Lu F, Imsabai W, Meir S, Reid MS. Silencing polygalacturonase expression inhibits tomato petiole abscission. J Exp Bot. 2008:**59**(4):973–979. https://doi.org/10.1093/jxb/ern023

Kalaitzis P, Koehler SM, Tucker ML. Cloning of a tomato polygalacturonase expressed in abscission. Plant Mol Biol. 1995:**28**(4):647–656. https://doi.org/10.1007/BF00021190

Kalaitzis P, Solomos T, Tucker ML. Three different polygalacturonases are expressed in tomato leaf and flower abscission, each with a different temporal expression pattern. Plant Physiol. 1997:**113**(4):1303–1308. https://doi.org/10.1104/pp.113.4.1303

Kim J. Four shades of detachment: regulation of floral organ abscission. Plant Signal Behav. 2014:**9**(11):e976154. https://doi.org/10.4161/15592324.2014.976154

Kim J, Shiu S-H, Thoma S, Li W-H, Patterson SE. Patterns of expansion and expression divergence in the plant polygalacturonase gene family. Genome Biol. 2006:**7**(9):R87–R87. https://doi.org/10.1186/gb-2006-7-9-r87

Konishi S, Izawa T, Lin SY, Ebana K, Fukuta Y, Sasaki T, Yano M. An SNP caused loss of seed shattering during rice domestication. Science. 2006:**312**(5778):1392–1396. https://doi.org/10.1126/science.1126410

Langfelder P, Horvath S. WGCNA: an R package for weighted correlation network analysis. BMC Bioinformatics. 2008:**9**(1):559–559. https://doi.org/10.1186/1471-2105-9-559

Lee Y, Yoon TH, Lee J, Jeon SY, Lee JH, Lee MK, Chen H, Yun J, Oh SY, Wen X, et al. A lignin molecular brace controls precision processing of cell walls critical for surface integrity in Arabidopsis. Cell. 2018:**173**(6):1468–1480.e9. https://doi.org/10.1016/j.cell.2018.03.060

Lers A, Sonego L, Green PJ, Burd S. Suppression of LX ribonuclease in tomato results in a delay of leaf senescence and abscission. Plant Physiol. 2006:**142**(2):710–721. https://doi.org/10.1104/pp.106.080135

Li F, Komatsu A, Ohtake M, Eun H, Shimizu A, Kato H. Direct identification of a mutation in *OsSh1* causing non-shattering in a rice (*Oryza sativa* L.) mutant cultivar using whole-genome resequencing. Sci Rep. 2020:**10**(1):1–13. https://doi.org/10.1038/s41598-020-71972-1

Li L-F, Olsen KM. To have and to hold: selection for seed and fruit retention during crop domestication. Curr Top Dev Biol. 2016:**119**:63–109. https://doi.org/10.1016/bs.ctdb.2016.02.002

Li Y-B, Yan M, Cui D-Z, Huang C, Sui X-X, Guo FZ, Fan Q-Q, Chu X-S. Programmed degradation of pericarp cells in wheat grains depends on autophagy. Front Genet. 2021:**12**:784545. https://doi.org/10.3389/fgene.2021.784545

Li C, Zhao M, Ma X, Wen Z, Ying P, Peng M, Ning X, Xia R, Wu H, Li J. Two cellulases involved in litchi fruit abscission are directly activated by an HD-Zip transcription factor LcHB2. J Exp Bot. 2019:**70**(19):5189–5203. https://doi.org/10.1093/jxb/erz276

Li C, Zhou A, Sang T. Rice domestication by reducing shattering. Science. 2006:**311**(5769):1936–1939. https://doi.org/10.1126/science.1123604

Li J, Zhu H, Yuan R. Profiling the expression of genes related to ethylene biosynthesis, ethylene perception, and cell wall degradation during fruit abscission and fruit ripening in apple. J Am Soc Hortic Sci. 2010:**135**(5):391–401. https://doi.org/10.21273/JASHS.135.5.391

Lin Z, Li X, Shannon LM, Yeh C-T, Wang ML, Bai G, Peng Z, Li J, Trick HN, Clemente TE, et al. Parallel domestication of the *Shattering1* genes in cereals. Nat Genet. 2012:**44**(6):720–724. https://doi.org/10.1038/ng.2281

Liu H, Fang X, Zhou L, Li Y, Zhu C, Liu J, Song Y, Jian X, Xu M, Dong L, et al. Transposon insertion drove the loss of natural seed shattering during foxtail millet domestication. Mol Biol Evol. 2022:**39**(6):msac078. https://doi.org/10.1093/molbev/msac078

Love MI, Huber W, Anders S. Moderated estimation of fold change and dispersion for RNA-seq data with DESeq2. Genome Biol. 2014:**15**(12):550. https://doi.org/10.1186/s13059-014-0550-8

Lowe K, Wu E, Wang N, Hoerster G, Hastings C, Cho M-J, Scelonge C, Lenderts B, Chamberlin M, Cushatt J, et al. Morphogenic regulators *Baby boom* and *Wuschel* improve monocot transformation. Plant Cell. 2016:**28**(9):1998–2015. https://doi.org/10.1105/tpc.16.00124

Lv S, Wu W, Wang M, Meyer RS, Ndjiondjop M-N, Tan L, Zhou H, Zhang J, Fu Y, Cai H, et al. Genetic control of seed shattering during African rice domestication. Nat Plants. 2018:**4**(6):331–337. https://doi.org/10.1038/s41477-018-0164-3

Mamidi S, Healey A, Huang P, Grimwood J, Jenkins J, Barry K, Sreedasyam A, Shu S, Lovell JT, Feldman M, et al. A genome resource for green millet *Setaria viridis* enables discovery of agronomically valuable loci. Nat Biotechnol. 2020:**38**(10):1203–1210. https://doi.org/10.1038/s41587-020-0681-2

Martin M. Cutadapt removes adapter sequences from high-throughput sequencing reads. Embnet J. 2011:**17**(1):10–12. https://doi.org/10.14806/ej.17.1.200

McCartney L, Marcus SE, Knox JP. Monoclonal antibodies to plant cell wall xylans and arabinoxylans. J Histochem Cytochem. 2005:**53**(4):543–546. https://doi.org/10.1369/jhc.4B6578.2005

McKim SM, Stenvik G-E, Butenko MA, Kristiansen W, Cho SK, Hepworth SR, Aalen RB, Haughn GW. The *BLADE-ON-PETIOLE* genes are essential for abscission zone formation in *Arabidopsis*. Development. 2008:**135**(8):1537–1546. https://doi.org/10.1242/dev.012807

Merelo P, Agustí J, Arbona V, Costa ML, Estornell LH, Gómez-Cadenas A, Coimbra S, Gómez MD, Pérez-Amador MA, Domingo C, et al. Cell wall remodeling in abscission zone cells during ethylene-promoted fruit abscission in citrus. Front Plant Sci. 2017:**8**:126. https://doi.org/10.3389/fpls.2017.00126

Mishra A, Khare S, Trivedi PK, Nath P. Ethylene induced cotton leaf abscission is associated with higher expression of cellulase (*GhCel1*) and increased activities of ethylene biosynthesis enzymes in abscission zone. Plant Physiol Bioch. 2008:**46**(1):54–63. https://doi.org/10.1371/journal.pone.0097652

Moll P, Ante M, Seitz A, Reda T. QuantSeq 3′ mRNA sequencing for RNA quantification. Nat Methods. 2014:**11**: i–iii. https://doi.org/10.1038/nmeth.f.376

Mookkan M, Nelson-Vasilchik K, Hague J, Zhang ZJ, Kausch AP. Selectable marker independent transformation of recalcitrant maize inbred B73 and sorghum P898012 mediated by morphogenic regulators *BABY BOOM* and *WUSCHEL2*. Plant Cell Rep. 2017:**36**(9):1477–1491. https://doi.org/10.1007/s00299-017-2169-1

Odonkor S, Choi S, Chakraborty D, Martinez-Bello L, Wang X, Bahri BA, Tenaillon MI, Panaud O, Devos KM. QTL Mapping combined with comparative analyses identified candidate genes for reduced shattering in *Setaria italica*. Front Plant Sci. 2018:**9**:918. https://doi.org/10.3389/fpls.2018.00918

Ogawa M, Kay P, Wilson S, Swain SM. ARABIDOPSIS DEHISCENCE ZONE POLYGALACTURONASE1 (ADPG1), ADPG2, and QUARTET2 are polygalacturonases required for cell separation during reproductive development in *Arabidopsis*. Plant Cell Online. 2009:**21**(1):216–233. https://doi.org/10.1105/tpc.108.063768

Patterson SE. Cutting loose. Abscission and dehiscence in Arabidopsis. Plant Physiol. 2001:**126**(2):494–500. https://doi.org/10.1104/pp.126.2.494

Phillips S. Flora of Ethiopia and Eritrea, vol. 7. Poaceae (Gramineae). Uppsala: National Herbarium, Addis Ababa University, Addis Ababa, Ethiopia and Department of Systematic Botany, Uppsala University; 1995.

Pourkheirandish M, Hensel G, Kilian B, Senthil N, Chen G, Sameri M, Azhaguvel P, Sakuma S, Dhanagond S, Sharma R, et al. Evolution of the grain dispersal system in barley. Cell. 2015:**162**(3):527–539.

Roberts JA, Elliott KA, Gonzalez-Carranza ZH. Abscission, dehiscence, and other cell separation processes. Annu Rev Plant Biol. 2002:**53**(1):131–158. https://doi.org/10.1146/annurev.arplant.53.092701.180236

Roberts JA, Whitelaw CA, Gonzalez-Carranza ZH, McManus MT. Cell separation processes in plants—models, mechanisms and manipulation. Ann Bot-London. 2000:**86**(2):223–235. https://doi.org/10.1006/anbo.2000.1203

Roongsattham P, Morcillo F, Fooyontphanich K, Jantasuriyarat C, Tragoonrung S, Amblard P, Collin M, Mouille G, Verdeil J-L, Tranbarger TJ. Cellular and pectin dynamics during abscission zone development and ripe fruit abscission of the monocot oil palm. Front Plant Sci. 2016:**7**:540. https://doi.org/10.3389/fpls.2016.00540

Roongsattham P, Morcillo F, Jantasuriyarat C, Pizot M, Moussu S, Jayaweera D, Collin M, Gonzalez-Carranza ZH, Amblard P, Tregear JW, et al. Temporal and spatial expression of polygalacturonase gene family members reveals divergent regulation during fleshy fruit ripening and abscission in the monocot species oil palm. BMC Plant Biol. 2012:**12**(1):150–150. https://doi.org/10.1186/1471-2229-12-150

Sanders PM, Bui AQ, Le BH, Goldberg RB. Differentiation and degeneration of cells that play a major role in tobacco anther dehiscence.

Sex Plant Reprod. 2005:**17**(5):219–241. https://doi.org/10.1007/s00497-004-0231-y

Senatore A, Trobacher CP, Greenwood JS. Ricinosomes predict programmed cell death leading to anther dehiscence in tomato. Plant Physiol. 2009:**149**(2):775–790. https://doi.org/10.1104/pp.108.132720

Shannon P, Markiel A, Ozier O, Baliga NS, Wang JT, Ramage D, Amin N, Schwikowski B, Ideker T. Cytoscape: a software environment for integrated models of biomolecular interaction networks. Genome Res. 2003:**13**(11):2498–2504. https://doi.org/10.1101/gr.1239303

Singh AP, Tripathi SK, Nath P, Sane AP. Petal abscission in rose is associated with the differential expression of two ethylene-responsive xyloglucan endotransglucosylase/hydrolase genes, *RbXTH1* and *RbXTH2*. J Exp Bot. 2011:**62**(14):5091–5103. https://doi.org/10.1093/jxb/err209

Tripathi SK, Singh AP, Sane AP, Nath P. Transcriptional activation of a 37 kDa ethylene responsive cysteine protease gene, *RbCP1*, is associated with protein degradation during petal abscission in rose. J Exp Bot. 2009:**60**(7):2035–2044. https://doi.org/10.1093/jxb/erp076

Tucker ML, Sexton R, del Campillo E, Lewis LN. Bean abscission cellulase characterization of a cDNA clone and regulation of gene expression by ethylene and auxin. Plant Physiol. 1988:**88**(4):1257–1262. https://doi.org/10.1104/pp.88.4.1257

VanBuren R, Wai CM, Wang X, Pardo J, Yocca AE, Wang H, Chaluvadi SR, Han G, Bryant D, Edger PP, et al. Exceptional subgenome stability and functional divergence in the allotetraploid Ethiopian cereal teff. Nat Commun. 2020:**11**(1):884. https://doi.org/10.1038/s41467-020-14724-z

van Doorn WG, Beers EP, Dangl JL, Franklin-Tong VE, Gallois P, Hara-Nishimura I, Jones AM, Kawai-Yamada M, Lam E, Mundy J, et al. Morphological classification of plant cell deaths. Cell Death Differ. 2011:**18**(8):1241–1246. https://doi.org/10.1038/cdd.2011.36

Wilson ZA, Song J, Taylor B, Yang C. The final split: the regulation of anther dehiscence. J Exp Bot. 2011:**62**(5):1633–1649. https://doi.org/10.1093/jxb/err014

Wimalanathan K, Lawrence-Dill CJ. Gene Ontology Meta Annotator for Plants (GOMAP). Plant Methods. 2021:**17**(1):54. https://doi.org/10.1186/s13007-021-00754-1

Wu X-M, Yu Y, Han L-B, Li C-L, Wang H-Y, Zhong N-Q, Yao Y, Xia G-X. The tobacco *BLADE-ON-PETIOLE2* gene mediates differentiation of the corolla abscission zone by controlling longitudinal cell expansion. Plant Physiol. 2012:**159**(2):835–850. https://doi.org/10.1104/pp.112.193482

Yamada T, Ichimura K, van Doorn WG. Relationship between petal abscission and programmed cell death in *Prunus yedoensis* and *Delphinium belladonna*. Planta. 2007:**226**(5):1195–1205. https://doi.org/10.1007/s00425-007-0566-3

Yoon J, Cho L, Kim SL, Choi H, Koh H, An G. The BEL1-type homeobox gene *SH5* induces seed shattering by enhancing abscission-zone development and inhibiting lignin biosynthesis. Plant J. 2014:**79**(5):717–728. https://doi.org/10.1111/tpj.12581

Yu Y, Hu H, Doust AN, Kellogg EA. Divergent gene expression networks underlie morphological diversity of abscission zones in grasses. New Phytologist. 2020a:**225**(4):1799–1815. https://doi.org/10.1111/nph.16087

Yu Y, Kellogg EA. Inflorescence abscission zones in grasses: diversity and genetic regulation. Annu Plant Rev. 2018:**1**(2): 497–532. https://doi.org/10.1002/9781119312994.apr0619

Yu Y, Leyva P, Tavares RL, Kellogg EA. The anatomy of abscission zones is diverse among grass species. Am J Bot. 2020b:**107**(4):549–561. https://doi.org/10.1002/ajb2.1454

Yu G, Wang L-G, Han Y, He Q-Y. Clusterprofiler: an R package for comparing biological themes among gene clusters. Omics J Integr Biology. 2012:**16**(5):284–287. https://doi.org/10.1089/omi.2011.0118

Zhao X, Xie W, Zhang J, Zhang Z, Wang Y. Histological characteristics, cell wall hydrolytic enzymes activity and candidate genes expression associated with seed shattering of *Elymus sibiricus* accessions. Front Plant Sci. 2017:**08**:606. https://doi.org/10.3389/fpls.2017.00606

Zhou Y, Lu D, Li C, Luo J, Zhu B-F, Zhu J, Shangguan Y, Wang Z, Sang T, Zhou B, et al. Genetic control of seed shattering in rice by the APETALA2 Transcription factor *SHATTERING ABORTION1*. Plant Cell. 2012:**24**(3):1034–1048. https://doi.org/10.1105/tpc.111.094383